© 2020. Published by The Company of Biologists Ltd | Journal of Cell Science (2020) 133, jcs245001. doi:10.1242/jcs.245001

RESEARCH ARTICLE

Mitofusin 2 but not mitofusin 1 mediates Bcl-XL-induced mitochondrial aggregation

Mengyan Du[1], Si Yu[1], Wenhua Su[1], Mengxin Zhao[2], Fangfang Yang[1], Yangpei Liu[1], Zihao Mai[1], Yong Wang[1], Xiaoping Wang[2,*] and Tongsheng Chen[1,*]

ABSTRACT

Bcl-2 family proteins, as central players of the apoptotic program, participate in regulation of the mitochondrial network. Here, a quantitative live-cell fluorescence resonance energy transfer (FRET) two-hybrid assay was used to confirm the homo-/hetero-oligomerization of mitofusins 2 and 1 (MFN2 and MFN1), and also demonstrate the binding of MFN2 to MFN1 with 1:1 stoichiometry. A FRET two-hybrid assay for living cells co-expressing CFP-labeled Bcl-XL (an anti-apoptotic Bcl-2 family protein encoded by *BCL2L1*) and YFP-labeled MFN2 or MFN1 demonstrated the binding of MFN2 or MFN1 to Bcl-XL with 1:1 stoichiometry. Neither MFN2 nor MFN1 bound with monomeric Bax in healthy cells, but both MFN2 and MFN1 bind to punctate Bax (pro-apoptotic Bcl-2 family protein) during apoptosis. Oligomerized Bak (also known as BAK1; a pro-apoptotic Bcl-2 family protein) only associated with MFN1 but not MFN2. Moreover, co-expression of Bcl-XL with MFN2 or MFN1 had the same anti-apoptotic effect as the expression of Bcl-XL alone to staurosporine-induced apoptosis, indicating the Bcl-XL has its full anti-apoptotic ability when complexed with MFN2 or MFN1. However, knockdown of MFN2 but not MFN1 reduced mitochondrial aggregation induced by overexpression of Bcl-XL, indicating that MFN2 but not MFN1 mediates Bcl-XL-induced mitochondrial aggregation.

KEY WORDS: MFN2, MFN1, Bcl-XL, Mitochondrial aggregation, FRET two-hybrid assay

INTRODUCTION

Mitochondria undergo continuous cycles between fission and fusion to maintain proper morphology and physiological functions, including ATP production (Brookes et al., 2004), mitochondrial DNA (mtDNA) maintenance (Wallace, 2005) and regulation of apoptosis (Jagasia et al., 2005; Wang and Youle, 2009). Dynamic mitochondrial behavior is believed to ensure appropriate mitochondrial distribution to provide ATP to localized cytosolic regions (Brookes et al., 2004). Frequent fusion and fission may be an efficient means of intermitochondrial DNA complementation through exchange of genomes between fusing mitochondria (Nakada et al., 2001). Mitochondrial fragmentation may participate in apoptosis (Olichon et al., 2002). Mitochondrial fusion defects result in fragmented mitochondria, and even participate in the pathogenesis of Charcot–Marie–Tooth disease type 2A (Züchner et al., 2004), whereas reduced mitochondrial fission leads to elongated, hyper-fused mitochondria and can delay caspase activation and cell death (Labbé et al., 2014; Karbowski et al., 2002; Sugioka et al., 2004; Breckenridge et al., 2003). Mitochondrial dynamics are regulated by a set of dynamin-related proteins. In mammalian cells, mitochondrial fission is mainly mediated by the GTPase dynamin-related protein 1 (Drp1; also known as DNM1L) (Smirnova et al., 2001), which is recruited from cytoplasm to mitochondria by several outer mitochondrial membrane (OMM) proteins [mitochondrial fission factor (MFF), Mid51 (MIEF1), Mid49 (MIEF2) and fission 1 protein (FIS1)] (Gandre-Babbe and van der Bliek, 2008; Palmer et al., 2011; James et al., 2003), assembling into a helical ring-like structure to 'drawstring' constrict mitochondria. Mitochondrial fusion involves OMM fusion and inner mitochondrial membrane (IMM) fusion. Although OMM fusion is highly coordinated with IMM fusion to maintain the integrity of organelles under normal conditions, they can also be uncoupled in cells (Labbé et al., 2014; Legros et al., 2002; Meeusen et al., 2004). Mitofusin 1 and 2 (MFN1 and MFN2), two dynamin-related GTPases embedded in the OMM, are essential for mitochondrial outer membrane fusion in mammalian cells (Santel and Fuller, 2001) while optic atrophy 1 (OPA1) mediates IMM fusion (Ishihara et al., 2006).

MFN1 and MFN2 are thought to promote mitochondrial fusion via forming homotypic and heterotypic oligomers and stimulating GTP hydrolysis (Chen et al., 2003; Koshiba et al., 2004). In 2004, the second C-terminal heptad-repeat domain (HR2) at N terminus of the mitofusins was identified as mediating the initial tethering of adjacent mitochondria by forming antiparallel dimers, while the GTPase domain is likely to provide biomechanical energy for full fusion (Koshiba et al., 2004). However, recent studies highlight that dimerization of GTPase domains, regulated by guanine nucleotide, is responsible for initial tethering, and disruption of GTPase domain dimerization abolishes the oligomerization ability of MFN1 (Cao et al., 2017; Qi et al., 2016). Although the molecular mechanism of oligomeric mitofusin formation is not clear and remains to be determined, there is no doubt about inhibitory roles of MFN1 or MFN2 on mitochondrial fragmentation in cells. Deletion of either MFN1 or MFN2 can not only induce mitochondrial fragmentation in cells and but also result in embryonic lethality in mice (Chen et al., 2003). Moreover, several studies have shown that mitochondrial fragmentation occurs during apoptosis (Jagasia et al., 2005; Goyal et al., 2007; Pinton et al., 2001; Fannjiang et al., 2004; Youle and Karbowski, 2005) and maintenance of mitochondrial fusion has been linked to protecting cells against apoptosis (Sugioka et al., 2004; Neuspiel et al., 2005).

Bcl-2 family proteins, as central players of the mitochondrion-dependent apoptotic program, participate in mitochondrial dynamic

[1]MOE Key Laboratory and Guangdong Provincial Key Laboratory of Laser Life Science, College of Biophotonics, South China Normal University, Guangzhou 510631, China. [2]Department of Pain Management, the First Affiliated Hospital, Jinan University, Guangzhou 510632, China.

*Authors for correspondence (txp2938@jnu.edu.cn; chentsh@scnu.edu.cn; chentsh126@126.com)

T.C., 0000-0002-9036-6676

Handling Editor: Jennifer Lippincott-Schwartz
Received 6 February 2020; Accepted 9 September 2020

Journal of Cell Science (2020) 133, jcs245001. doi:10.1242/jcs.245001

regulation (Gross and Katz, 2017). Bcl-2 family proteins are normally divided into multidomain antiapoptotic Bcl-2, Bcl-XL (encoded by *BCL2L1*) and Mcl-1, multidomain pro-apoptotic Bax and Bak (also known as BAK1), and pro-apoptotic BH3-only proteins (Chen et al., 2015). Antiapoptotic proteins (Bcl-2, Bcl-XL and Mcl-1) preserve mitochondrial integrity to inhibit cells apoptosis mainly through inhibiting activation of pro-apoptotic proteins, and Bcl-XL has a stronger effect in preventing apoptosis than Bcl-2 and Mcl-1 owing to its dual inhibition of pro-apoptotic Bax and Bak as well as higher protein stability (Chen et al., 2015; Willis et al., 2005; Hockings et al., 2018). Apoptotic stimuli activate Bax and Bak to coalesce on the surface of the OMM, and form large foci, which are responsible for mitochondrial outer membrane permeabilization (MOMP) (Chen et al., 2015) and culminate in release of cytochrome *c* into the cytosol, subsequent caspase activation and apoptosis. In addition to their apoptotic role, Bax and Bak colocalize with DRP1 and MFN2 at prospective mitochondrial fission sites during apoptosis (Nechushtan et al., 2001; Valentijn et al., 2003; Karbowski et al., 2002; Youle and Karbowski, 2005). Quantification of mitochondrial dynamics by photolabeling of mitochondrial matrix shows that mitochondrial fusion is blocked during the Bax activation phase of apoptosis independently from caspase activation (Karbowski et al., 2004). In 2006, Karbowski et al. demonstrated that Bax or Bak is required for normal fusion of mitochondria into elongated tubules in healthy cells (Karbowski et al., 2006), and Bax seems to induce activation of MFN2. Moreover, another study shows that Bak interacts with MFN1 and MFN2 (Brooks et al., 2007) in healthy HeLa cells, using co-immunoprecipitation (co-IP) assay and acceptor photobleaching-based fluorescence resonance energy transfer (FRET) measurements, but during apoptosis, Bak dissociates from MFN2 and enhances the association with MFN1, as shown by a co-IP assay. Indeed, it has been demonstrated in an *in vitro* experiment system of mitochondrial fusion, that the soluble form of Bax positively regulates mitochondrial fusion exclusively through homotypic MFN2 trans complexes (Hoppins et al., 2011). Interestingly, Bcl-XL may tip the balance in favor of fusion or fission depending on the relative Bcl-XL expression level (Delivani et al., 2006; Sheridan et al., 2008). Expression of Bcl-XL in HeLa cells produced two distinct mitochondrial phenotypes including aggregated mitochondria (mitochondrial clustering in the perinuclear region) and fragmented mitochondria: aggregated mitochondria increased but fragmented mitochondria decreased with increasing Bcl-XL (Delivani et al., 2006; Sheridan et al., 2008). However, Mcl-1 failed to perturb mitochondrial networks in HeLa cells at any of the plasmid concentrations tested (Sheridan et al., 2008). Previous reports also showed that addition of purified recombinant full-length monomeric soluble Bcl-XL can stimulate mitochondrial fusion in a dose-dependent manner (Hoppins et al., 2011). This finding is consistent with the observation that overexpression of Bcl-XL increases mitochondrial connectivity in cells. An *in vitro* GTPase assay with purified recombinant full-length Bcl-XL and full-length human Drp1 showed that Bcl-XL increased Drp1 GTPase activity (Li et al., 2008). Bcl-XL selectively co-immunoprecipitated MFN2 but not MFN1 or OPA1 in HEK293T cells (Delivani et al., 2006). However, co-IP experiments showed that Bcl-XL binds to both MFN1 and MFN2 in HeLa cells (Cleland et al., 2011) and a Bcl-XL–Bax chimera [containing helix 5 (H5) of Bax replacing H5 of Bcl-XL (denoted Bcl-XL/Bax H5)] binds to mitofusins better than to either wild-type Bax or Bcl-XL and this chimera can induce substantial mitochondrial fragmentation in healthy cells (Cleland et al., 2011).

In this report, we performed live-cell FRET to explore the regulation between mitofusins and Bcl-XL. A FRET two-hybrid assay in living HeLa cells co-expressing CFP–Bcl-XL together with YFP–MFN2 or YFP–MFN1 verified the hetero-oligomerization between mitofusins and Bcl-XL, with MFN2– or MFN1–Bcl-XL formed in complexes with 1:1 stoichiometry. Live-cell FRET analysis also showed that GTPase domain mutants of MFN2 and MFN1 still had the ability to form oligomers, but lose the ability to bind to Bcl-XL, indicating that GTPase domains of MFN2 and MFN1 may play key roles in binding to Bcl-XL. Co-expression of Bcl-XL and MFN2 or MFN1 had the same anti-apoptotic effect as the expression of Bcl-XL alone against staurosporine (STS) treatment, demonstrating that Bcl-XL complexed with MFN2 or MFN1 maintains an anti-apoptotic function. However, knockdown of MFN2 but not MFN1 significantly reduced mitochondrial aggregation induced by overexpressed Bcl-XL, indicating that Bcl-XL-induced mitochondrial aggregation is probably mediated by MFN2.

RESULTS

Subcellular localization of MFN2 and MFN1

To visualize the subcellular localization of MFN2 and MFN1, YFP–MFN2 and YFP–MFN1 as well as YFP (control) were transfected, respectively, in living HeLa cells. At 24 h after transfection, mitochondria were stained by using Mitotracker Deep Red 633 dye and cells subsequently were imaged by using our Zeiss Apotome.2 imaging system. As shown in Fig. 1A, fluorescence images showed that YFP was distributed evenly in cells, while YFP–MFN2 and YFP–MFN1 were colocalized with mitochondria. Regions within white dotted lines were chosen for Pearson correlation analysis to quantify the distributions of YFP–MFN2, YFP–MFN1 and YFP, and the corresponding fluorescence intensity scatter graph and Pearson correlation coefficient (R_r) between YFP or YFP-tagged MFN2 and MFN1 and Mitotracker are shown in the right-hand panels of Fig. 1A. R_r for the representative cells expressing YFP–MFN2 or YFP–MFN1 was 0.45 or 0.38, much higher than the −0.25 for R_r for cells expressing YFP, showing that MFN2 and MFN1 are partially colocalized with the mitochondria. Statistical R_r values between YFP, YFP–MFN2 or YFP–MFN1 and the corresponding mitochondria were −0.18±0.08, 0.50±0.08 or 0.29±0.19, respectively (Fig. 1B), confirming that both MFN2 and MFN1 localize to mitochondria.

Mitochondria in the cells expressing YFP were tubular (Fig. 1A, upper panel), while mitochondria of the cells expressing YFP–MFN2 or YFP–MFN1 were aggregated (Fig. 1A, middle and lower panel); the corresponding statistical results on mitochondrial morphology from 100 cells are shown in Fig. 1C. Approximately 93% or 94% of the cells transfected with 200 ng or 400 ng of YFP–MFN2 exhibited aggregated mitochondria, and ∼77% or 87% of the cells transfected with 200 or 400 ng of YFP–MFN1 exhibited aggregated mitochondria, while the cells transfected with 200 or 400 ng of YFP exhibited 83% of tubular mitochondria and only 9% or 8% of aggregated mitochondria, indicating that both MFN2 and MFN1 can induce mitochondrial aggregation.

Homo- and hetero-oligomerization of MFN2 and MFN1

Quantitative FRET analysis was performed on our Zeiss Apotome.2 imaging system to quantify the homo-oligomerization of MFN2 and MFN1 in living cells co-expressing CFP–MFN2 plus YFP–MFN2, and CFP–MFN1 plus YFP–MFN1. To avoid potential false-positive results, cells co-expressing CFP plus YFP, CFP–MFN2 plus YFP–ActA (mitochondria-specific Act-A tail-anchor

Journal of Cell Science (2020) 133, jcs245001. doi:10.1242/jcs.245001

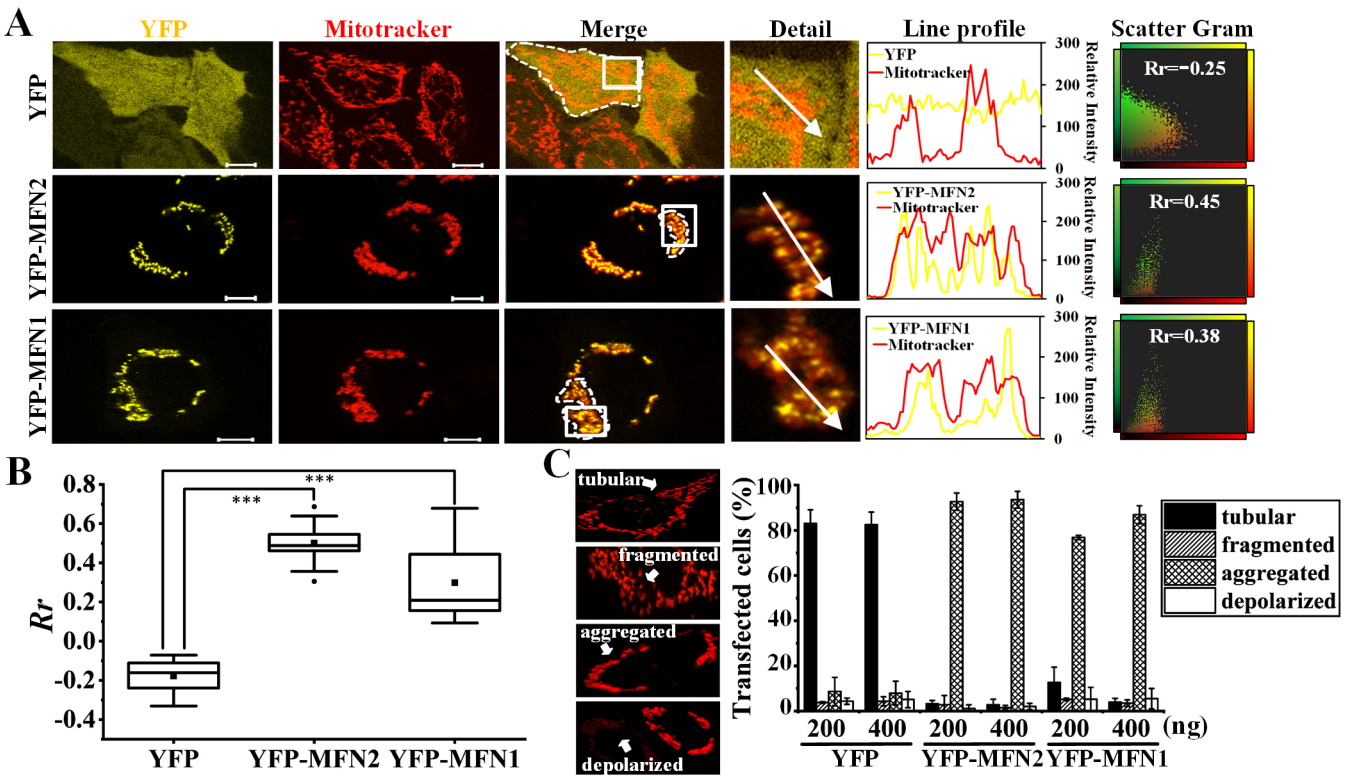

Fig. 1. Mitochondrial localization of MFN2 and MFN1. (A) Fluorescence images of representative living HeLa cells expressing YFP, YFP–MFN2 and YFP–MFN1. Cells were stained with Mitotracker Deep Red 633. Detail panels show information from the white boxes in the merge images, and intensity line profiles show the fluorescence intensities of YFP and Mitotracker along the white arrows in the merge panels. Regions within the white dotted line in the merge images were chosen for Pearson correlation analysis, and the corresponding scatter diagram and Pearson correlation coefficient (R_r) between mitochondria and YFP, MFN2 or MFN1 are shown in the right panels. Scale bars: 10 µm. (B) Mean R_r values for the colocalization between mitochondria and YFP, MFN2 or MFN1 in cells expressing YFP, YFP–MFN2 or YFP–MFN1. n=20 cells each. The box represents the 25–75th percentiles, and the median is indicated by the line and the mean by a square symbol. The whiskers show the maximum and minimum values. ***P<0.001 (two-tailed Student's t-test). (C) Percentages of cells with indicated mitochondrial morphologies in YFP-positive cells transfected with the indicated amounts of plasmids. 100 cells were scored for each experiment, and data were collected from three independent experiments. Data represent mean±s.d.

sequence, ActA is a control protein that does not bind to MFN2 or MFN1; Aranovich et al., 2012; Zhu et al., 1996), and CFP–MFN1 plus YFP–ActA were used as negative samples. We also evaluated colocalization between CFP and YFP-tagged MFN2 and MFN1 (Fig. S2A,B), and performed a co-IP assay between CFP and MFN1 by using cells co-expressing CFP plus MFN1–Myc (Myc tag on the C-terminus of MFN1) (Fig. S2C). Pearson correlation analysis (R_r) showed that CFP did not colocalize to MFN2 or MFN1, and co-IP assay further confirmed that CFP does not bind to MFN1. Fig. 2A shows the fluorescence images (DD, DA, AA, where D represents donor and A acceptor) of cells co-expressing CFP plus YFP (control), CFP–MFN2 plus YFP–ActA (control), CFP–MFN1 plus YFP–ActA (control), CFP–MFN2 plus YFP–MFN2, and CFP–MFN1 plus YFP–MFN1, respectively, and the corresponding pixel-to-pixel pseudo-color donor-centric FRET efficiency (E_D) and acceptor-centric FRET efficiency (E_A) as well as the concentration ratio (R_C) of total acceptor-to-donor images. Pixel-to-pixel E_D, E_A and R_C values from 30 cells were binned with 0.01 bin size of R_C, and the corresponding E_D–R_C and E_A–$1/R_C$ plots are shown in Fig. 2B. The E_D or E_A values of cells co-expressing CFP plus YFP, and CFP–MFN2 or CFP–MFN1 plus YFP–ActA were all lower than 0.05 in the 0–4 range for R_C or $1/R_C$, while E_D or E_A values increased with R_C or $1/R_C$, and tended to be ∼0.4 for the cells co-expressing CFP–MFN2 plus YFP–MFN2 and ∼0.2 for the cells co-expressing CFP–MFN1 plus YFP–MFN1 when R_C or $1/R_C$ was larger than 2. E_D and E_A values for the cells co-expressing CFP–MFN2 plus YFP–MFN2, or CFP–MFN1 plus YFP–MFN1 were significantly higher than that of the cells co-expressing CFP plus YFP, or CFP–MFN2 or CFP–MFN1 plus YFP–ActA in the 0–4 range for R_C, demonstrating that both MFN2 and MFN1 can form homotypic oligomers.

To inspect hetero-oligomerization of MFN2 and MFN1, cells were co-transfected with CFP–MFN1 plus YFP–MFN2. Fluorescence images showed that MFN2 colocalized strongly with MFN1 (Fig. 2C), which was further confirmed by the high R_r value, with a mean of 0.76 between MFN2 and MFN1 (Fig. 2D). Quantitative FRET two-hybrid assay was used to further quantify the hetero-oligomerization of MFN2 and MFN1. The fluorescence images (DD and AA) of representative cells co-expressing CFP–MFN1 plus YFP–MFN2, and the corresponding pixel-to-pixel pseudo-color E_D and E_A as well as R_C images were shown in Fig. 2E. The E_D, E_A and R_C values from 60 cells (with bin size of 0.01 for R_C) are shown in E_D–R_C and E_A–$1/R_C$ plots (Fig. 2F). E_D or E_A rapidly increased with R_C or $1/R_C$, and tended to be a stable value when R_C was larger than 2. E_{Amax} and E_{Dmax} can be estimated by finding the best binding curves (Fig. 2F, red lines) during the fitting procedure according to Eqn 5 and 6 (see Materials and Methods). Therefore, the stoichiometry ratio (v, n_D/n_A) of MFN1 to MFN2 according to Eqn 7 obtained from the ratio of E_{Amax} to E_{Dmax} was 1.06 (Fig. 2F). Statistical v values from three independent

Journal of Cell Science (2020) 133, jcs245001. doi:10.1242/jcs.245001

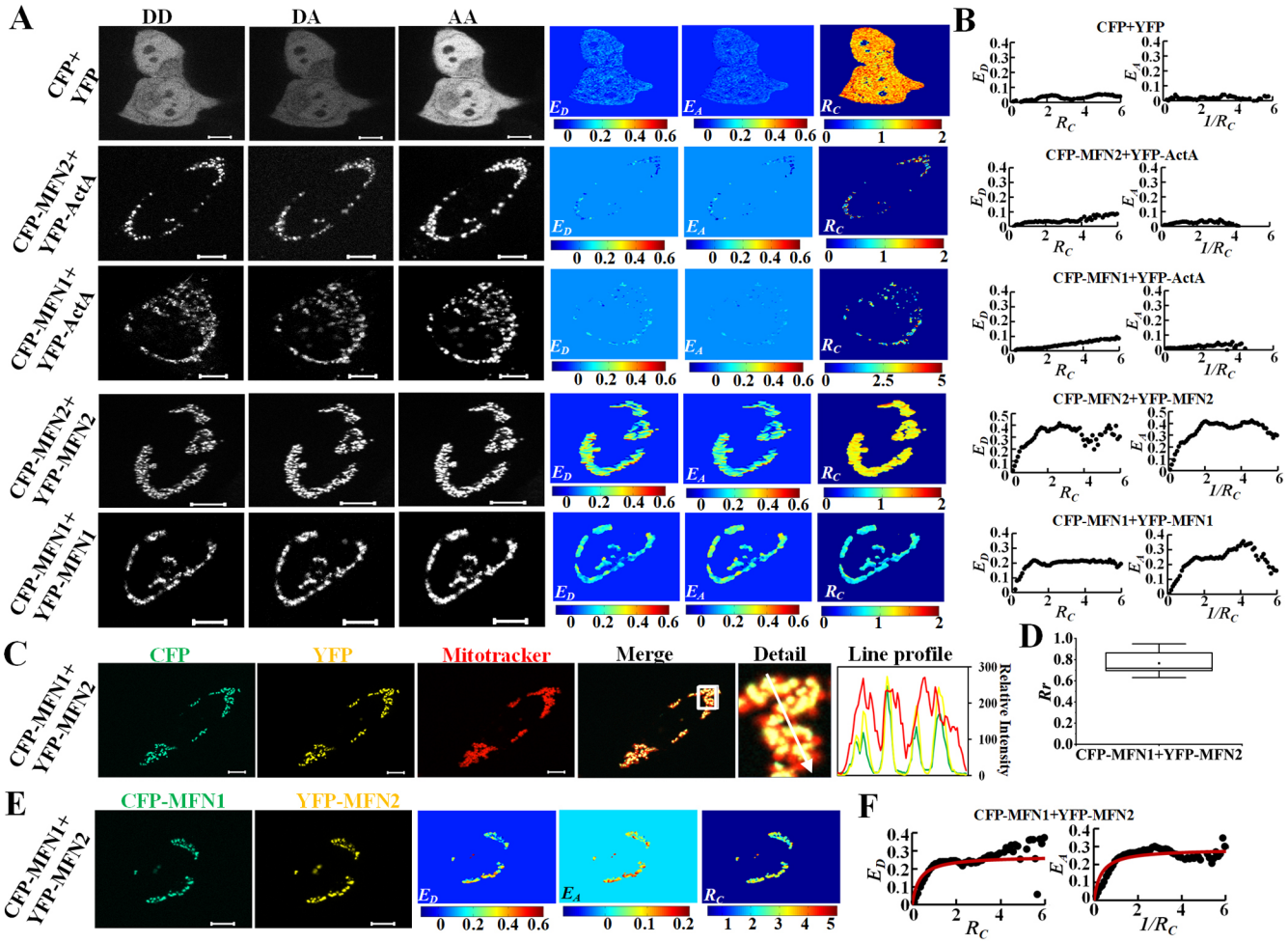

Fig. 2. Homo- and hetero-oligomerization of MFN2 and MFN1. (A) Three fluorescence images (DD, DA, and AA) of representative living cells separately co-expressing CFP+YFP (control), CFP–MFN2 or –MFN1+YFP–ActA (control), CFP–MFN2+YFP–MFN2, and CFP–MFN1+YFP–MFN1, and the corresponding pixel-to-pixel pseudo-color E_D and E_A as well as R_C images. Scale bars: 10 µm. (B) E_D–R_C and E_A–$1/R_C$ plots (0.01 bin size for R_C) from 30 cells co-expressing indicated plasmids. (C) Similar images to A for living cells co-expressing CFP–MFN1+YFP–MFN2. Cells were stained with Mitotracker. Line profiles show the fluorescence intensities of CFP, YFP and Mitotracker along the selected white arrows in the merge panels. Scale bars: 10 µm. (D) R_r values for the colocalization between MFN1 and MFN2. The box represents the 25–75th percentiles, and the median is indicated by the line and the mean by a square symbol. The whiskers show the maximum and minimum values. n=20 cells. (E) Fluorescence images (DD and AA) of representative living cells separately co-expressing CFP–MFN1+YFP–MFN2, and the corresponding pixel-to-pixel pseudo-color E_D and E_A as well as R_C images. Scale bars: 10 µm. (F) E_D–R_C and E_A–$1/R_C$ plots from at least 60 cells co-expressing CFP–MFN1+YFP–MFN2. Red lines represent the best fitted curves of data from cells co-expressing CFP–MFN1+YFP–MFN2.

experiments were 1.15±0.1 (mean±s.d.), implying that MFN1 binds to MFN2 mainly with 1:1 stoichiometry. Live-cell FRET analysis also showed that GTPase domain mutants of MFN2 [MFN2(K109A); alanine replacement of the lysine at residue 109 (K109A)] and MFN1 [MFN1(K88T), threonine replacement of the lysine at residue 88 (K88T)] still have the ability of forming homo- or hetero-oligomers (Fig. S3).

MFN2 and MFN1 both bind to Bcl-XL with 1:1 stoichiometry

To detect whether MFN2 or MFN1 colocalized with Bcl-XL in living cells, cells were co-transfected with CFP–Bcl-XL plus YFP–MFN2, or CFP–Bcl-XL plus YFP–MFN1, respectively, for 24 h, and stained by using Mitotracker Deep Red 633 dye before fluorescence imaging using our system. As shown in Fig. 3A, Bcl-XL was observed in mitochondria and cytosol, while MFN2 or MFN1 still localized to mitochondria. We chose mitochondrial regions for further Pearson correlation analysis between YFP–MFN2 or YFP–MFN1 and CFP–Bcl-XL. The mean±s.d. R_r value (Fig. 3B) from 30 mitochondria (each mitochondrion from a different cell) was 0.49±0.1 for the cells co-expressing YFP–MFN2 plus CFP–Bcl-XL and was 0.54±0.11 for cells co-expressing YFP–MFN1 plus CFP–Bcl-XL, indicating that both MFN2 and MFN1 co-localize with Bcl-XL on mitochondria.

We next performed FRET two-hybrid assay for cells co-transfected with CFP–Bcl-XL plus YFP–MFN2 or YFP–MFN1 to resolve the stoichiometry between MFN2 or MFN1 and Bcl-XL. The fluorescence images of representative cells co-expressing the indicated plasmids and the corresponding pixel-to-pixel pseudo-color E_D and E_A as well as R_C images are shown in Fig. 3C. Fig. 3D shows the E_D–R_C and E_A–$1/R_C$ plots from 60 cells, and mean±s.d. v values from three independent experiments were 1.15±0.2 for Bcl-XL to MFN2, and 1.28±0.23 for the Bcl-XL to MFN1, implying that both MFN2 and MFN1 can bind to Bcl-XL to form heterotypic oligomers, and MFN2 or MFN1 binds to Bcl-XL mainly with a 1:1 stoichiometry. Live-cell FRET analysis also showed that GTPase

Journal of Cell Science (2020) 133, jcs245001. doi:10.1242/jcs.245001

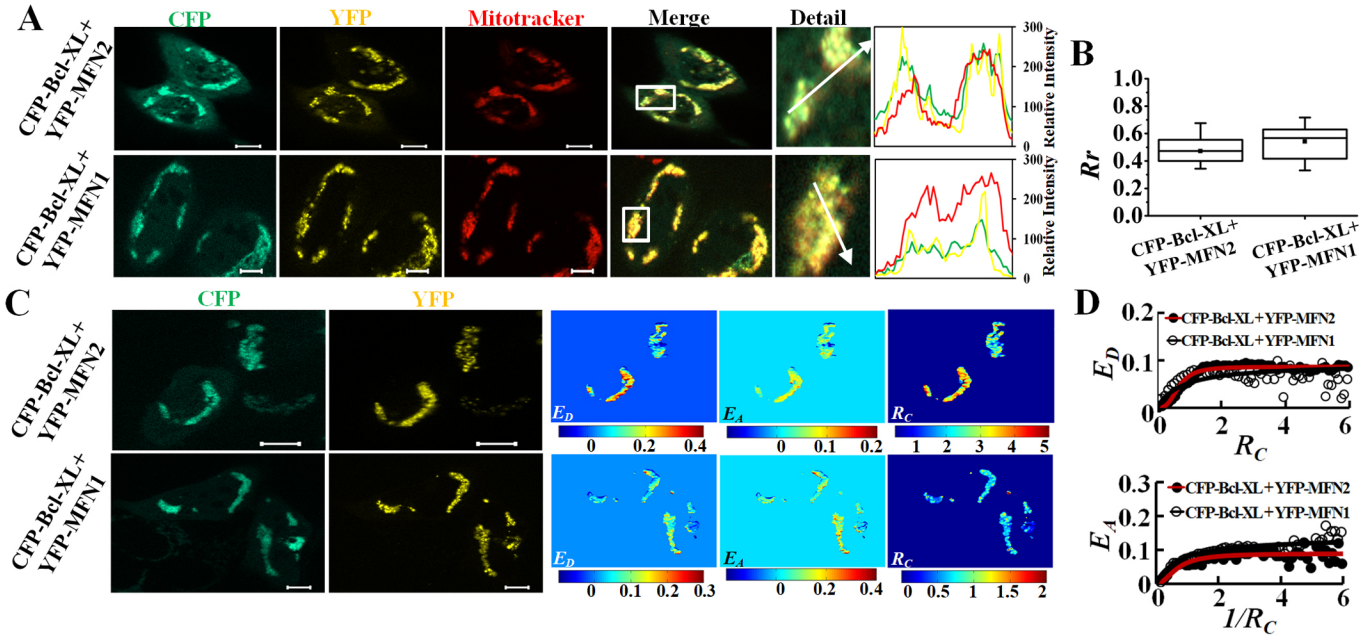

Fig. 3. MFN2 and MFN1 bind to Bcl-XL with 1:1 stoichiometry. (A) Fluorescence images of representative living HeLa cells co-expressing CFP–Bcl-XL+YFP–MFN2, and CFP–Bcl-XL+YFP–MFN1, respectively. Cells were also stained with Mitotracker. Detail panels show information from white boxes in the merge images, and intensity line profiles show the fluorescence intensities of CFP, YFP and Mitotracker along the white arrows in the merge panels. Scale bars: 10 µm. (B) R_r values for the colocalization between Bcl-XL and MFN2 and MFN1. The box represents the 25–75th percentiles, and the median is indicated by the line and the mean by a square symbol. The whiskers show the maximum and minimum values. n=20 cells each. (C) Fluorescence images (DD and AA) of representative living cells separately co-expressing CFP–Bcl-XL+YFP–MFN2 or YFP–MFN1, and the corresponding pixel-to-pixel pseudo-color E_D and E_A as well as R_C images. Scale bars: 10 µm. (D) E_D–R_C and E_A–$1/R_C$ plots for cells co-expressing CFP–Bcl-XL+YFP–MFN2 or YFP–MFN1. n=60 cells each. Red lines represent the best fitted curves of data from cells co-expressing CFP–Bcl-XL+YFP–MFN2. Black lines represent fitted curves of data from cells co-expressing CFP–Bcl-XL+YFP–MFN1.

domain mutants MFN2(K109A) MFN1(K88T) lose the ability to bind with Bcl-XL (Fig. S4), indicating that GTPase domains of MFN2 and MFN1 may play key roles in binding with Bcl-XL. In contrast to our FRET assay, a co-IP assay showed that Bcl-XL co-immunoprecipitated with not only MFN1 but also MFN2(K109A) and MFN1(K88T) (Fig. S4).

MFN2 but not MFN1 mediates Bcl-XL-induced mitochondrial aggregation

To assess whether the binding of MFN2 to Bcl-XL is responsible for Bcl-XL-induced mitochondrial aggregation, we firstly knocked down MFN2 in HeLa cells by using small interfering RNAs (siRNA). Cells were transfected without [control, (−)] or with scrambled siRNA (negative control, siCtrl), or with MFN2 siRNA (siMFN2) for 48 h, and the silencing efficiency was over 70% (Fig. 4A). Secondly, we further used our imaging system to examine the effect of MFN2 silencing on mitochondrial morphology. Mitotracker Deep Red 633 dye was used to label mitochondria. Statistical results from three independent experiments (100 cells for each experiment) showed that ∼61% of cells exhibited mitochondrial fragmentation in siMFN2 cells, but only 8% or 7% of cells had mitochondrial fragmentation in siCtrl or (−) cells (Fig. 4C), confirming that MFN2 mediates mitochondria fusion. Finally, in order to evaluate the effect of MFN2 silencing on Bcl-XL-induced mitochondrial aggregation, after cells were transfected with siCtrl or siMFN2 for 24 h, cells were re-transfected without (control) or with CFP–Bcl-XL for another 24 h, and then stained with Mitotracker for 30 min before imaging. Statistical results from three independent experiments (100 cells for each experiment) are shown in Fig. 4D. In cells transfected with siCtrl and 1000 ng of CFP, ∼11% of the cells expressing CFP exhibited aggregated mitochondria, while 50% of the cells transfected with siCtrl and 1000 ng of CFP–Bcl-XL exhibited aggregated mitochondria. However, when cells were transfected with siMFN2 and the same quality of CFP–Bcl-XL, only 31% of cells exhibited mitochondrial aggregation. These data confirm that overexpressed Bcl-XL can induce aggregation of mitochondria in which MFN2 plays an important role.

Similarly, we also investigated whether MFN1 is responsible for Bcl-XL-induced mitochondrial aggregation. We also knocked down MFN1 in HeLa cells by using siRNA, and the efficiency of MFN1 silencing was over 70% (Fig. 4B). Results of mitochondrial fluorescence imaging showed that about 73% of the cells transfected with siMFN1 exhibited short/fragment mitochondria. Only 18% or 14% of the cells transfected with siCtrl or (−) had fragment mitochondria (Fig. 4E). These data confirm that knocking down MFN1 induces mitochondrial fragmentation. Next, we also evaluate the effect of MFN1 silencing on Bcl-XL-induced mitochondrial aggregation. Results from three independent experiments showed that the proportion of cells with aggregated mitochondria was ∼45% for the cells expressing Bcl-XL and transfected with siCtrl. Interestingly, the proportion of cells with aggregated mitochondria was still ∼44% for the expressing Bcl-XL and transfected with siMFN1 (Fig. 4F). We thus reason that MFN1 is not responsible for Bcl-XL-induced mitochondrial aggregation.

Neither MFN2 nor MFN1 alters the anti-apoptotic ability of Bcl-XL

Based on the finding that MFN2 and MFN1 directly bind to Bcl-XL to form hetero-oligomers (Fig. 3), we further evaluated

Journal of Cell Science (2020) 133, jcs245001. doi:10.1242/jcs.245001

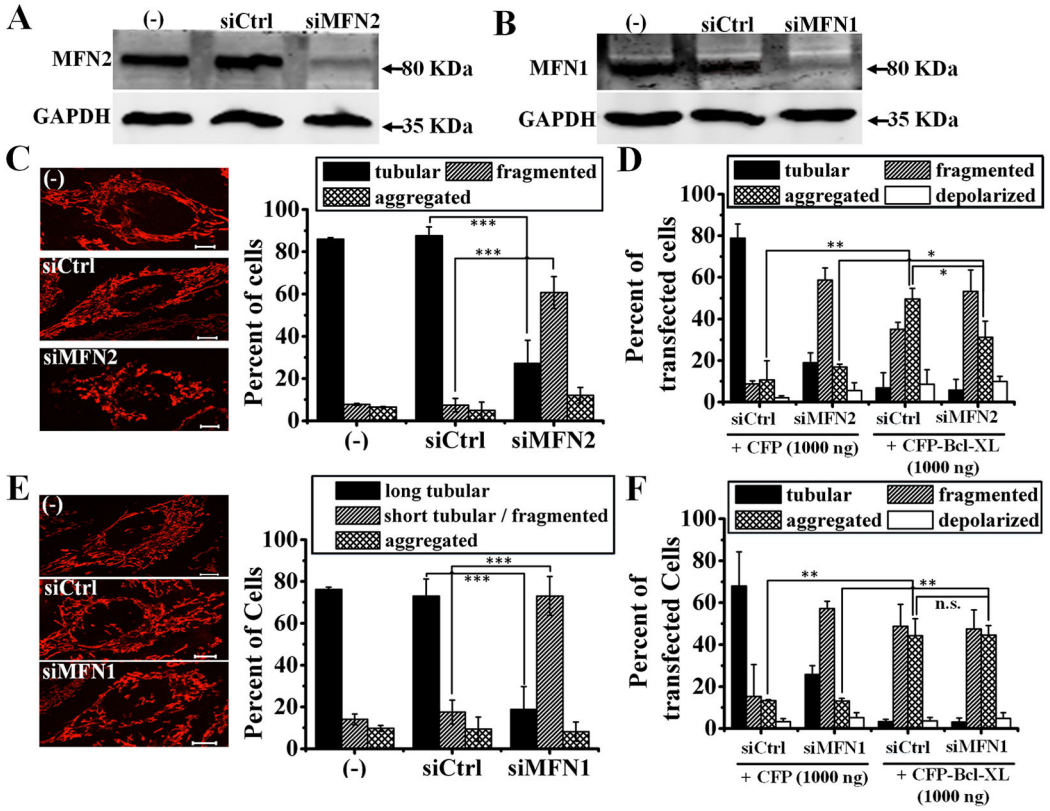

Fig. 4. MFN2 but not MFN1 mediates mitochondrial aggregation induced by overexpressed Bcl-XL. (A) Immunoblots for cells transfected with (–), scrambled siRNA (siCtrl) or MFN2 siRNA (siMFN2) for 48 h. (B) Immunoblots for cells transfected with (–), siCtrl or MFN1 siRNA (siMFN1) for 48 h. (C,E) Representative fluorescence images (left panels) of cells transfected with indicated siRNA for 48 h and stained with Mitotracker, and percentages of cells (right panel) with indicated mitochondrial morphologies. Scale bars: 10 µm. (D,F) Percentages of cells with indicated mitochondrial morphologies in the cells co-transfected with the indicated siRNA for 24 h and then re-transfected with indicated plasmids for another 24 h. For B,C,E and F, data were collected from three independent experiments (n=100 cells each). Data are mean±s.d. ***P<0.001, **P<0.01, *P<0.05, n.s. (not significant), P>0.05 (two-tailed Student's t-test).

whether MFN2 and/or MFN1 altered the anti-apoptotic activity of Bcl-XL. Cells were co-transfected with CFP plus YFP, CFP plus YFP–MFN2, CFP plus YFP–MFN1, CFP–Bcl-XL plus YFP, CFP–Bcl-XL plus YFP–MFN2, and CFP–Bcl-XL plus YFP–MFN1, respectively. At 24 h after transfection, cells were treated without (control) or with STS for 5 h, and then stained by using DilC1(5) (a membrane potential-dependent dye; lack of staining represents no membrane potential) and Hoechst 33258 (a nuclear staining dye) for 30 min before fluorescence imaging. Fig. 5A shows the images of representative cells co-expressing CFP plus YFP, CFP plus YFP–MFN2, CFP plus YFP–MFN1, CFP–Bcl-XL plus YFP, CFP–Bcl-XL plus YFP–MFN2, and CFP–Bcl-XL plus YFP–MFN1, respectively. In the control cells, all the co-transfections did not induce obvious loss of mitochondrial membrane potential [negative for DilC1(5) staining] or nuclei condensation (cell death) (Fig. 5A–C). In STS-treated cells, 93% of cells co-expressing CFP plus YFP were negative for DilC1(5) and apoptosis, while only 30% of cells co-expressing CFP–Bcl-XL plus YFP exhibited apoptosis, demonstrating the anti-apoptotic action of Bcl-XL. Approximately 90% of the STS-treated cells co-expressing CFP–MFN2 plus YFP were negative for DilC1(5) and apoptosis, while ∼27% and ∼35% of the STS-treated cells co-expressing CFP–Bcl-XL plus YFP–MFN2 were negative for DilC1(5) and apoptosis, respectively, implying that Bcl-XL maintains its full anti-apoptotic ability in the presence of MFN2. Similarly, in the STS-treated cells, ∼97% and ∼95% cells co-expressing CFP–MFN1 plus YFP were negative for DilC1(5) and apoptosis, respectively, cells, while ∼35% and ∼38% of the STS-treated cells co-expressing CFP-Bcl-XL plus YFP–MFN1 were negative for DilC1(5) and apoptosis, respectively, implying that Bcl-XL maintains its full anti-apoptotic ability in the presence of MFN1.

Interactions between MFN2 and MFN1 and other Bcl-2 family proteins

We also studied the interactions between MFN2 and MFN1 and the pro-apoptotic proteins Bax and Bak, and anti-apoptotic Mcl-1 in the same way. To research colocalization of MFN2 or MFN1 with Bax in healthy (control) or apoptosis cells, cells co-transfected with CFP-Bax and YFP–MFN2 or YFP–MFN1 for 24 h were treated without (control) or with STS for 4 h, and then stained by using DilC1(5) for 30 min before fluorescence imaging. Our previous report (Yang et al., 2019) has proved that STS indeed induced Bax translocation from cytosol to mitochondria and subsequent Bax cluster formation. In contrast to the uniform distribution of CFP–Bax in control cells (Fig. 6A, upper panel), CFP–Bax distributes to punctuate clusters in STS-treated cells (Fig. 6A, upper panel) and partially colocalized with YFP–MFN2. Similarly, CFP–Bax clusters also partially colocalized with YFP–MFN1 (Fig. 6A, lower panel). Pearson correlation analysis showed that R_r values (Fig. 6B) between CFP–Bax and YFP–MFN2, or CFP–Bax and YFP–MFN1 were 0.12±0.06 or 0.10±0.07 in control cells, but were 0.57±0.13 or 0.50±0.15 in STS-treated cells, suggesting that MFN2 or MFN1 colocalizes with Bax in apoptotic cells rather than healthy cells.

Journal of Cell Science (2020) 133, jcs245001. doi:10.1242/jcs.245001

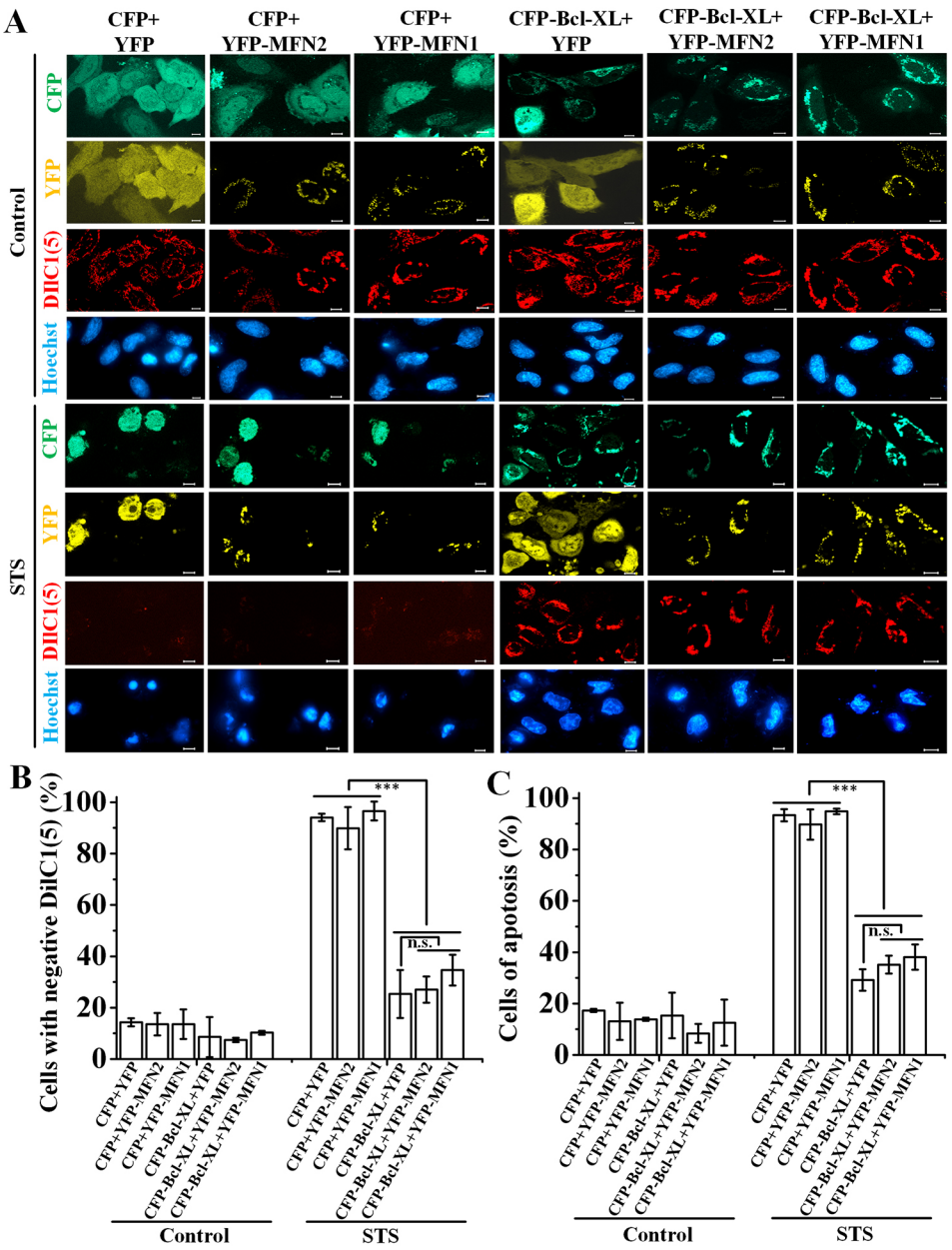

Fig. 5. Neither MFN2 nor MFN1 alter the anti-apoptotic ability of Bcl-XL. (A) Fluorescence images of cells co-expressing CFP+YFP, CFP+YFP–MFN2, CFP+YFP–MFN1, CFP–Bcl-XL+YFP, CFP–Bcl-XL+YFP–MFN2, and CFP–Bcl-XL+YFP–MFN1 in absence (Control) or presence of STS (2 µM, 5 h), respectively. Mitochondria were stained with DilC1(5) to detect changes in mitochondrial membrane potential and nuclei were stained with Hoechst to visualize changes in nuclear morphology. Scale bars: 10 µm. (B) Quantification of the percentage of cells with a lack of a mitochondrial membrane potential difference as revealed by lack of DilC1(5) staining. (C) Quantification of the percentage of apoptotic cells with nuclei condensation. For B and C, data were collected from three independent experiments (n=100 cells each). Data represent mean±s.d. ***P<0.001, n.s. (not significant), P>0.05 (two-tailed Student's t-test).

We further analyzed interactions between MFN2 and MFN1 and Bax using quantitative FRET analysis. Fig. 4C showed representative fluorescence images of cells co-expressing CFP–Bax and YFP–MFN2, or CFP–Bax and YFP–MFN1 in control cells and STS-treated cells, and the corresponding pixel-to-pixel pseudo-color E_D and E_A as well as Rc images. E_D values in the 0–6 range of R_C or E_A values in the 0–6 range of $1/R_C$ between both MFN2 and MFN1 and Bax in control cells were about 0, much lower than that in STS-treated cells (Fig. 6D), further confirming that MFN2 and MFN1 can only bind with clustering Bax and not monomeric Bax. We next assessed the stoichiometry of Bax and MFN1 in apoptosis cells by using FRET two-hybrid assay. Results from three independent experiments (62 cells for each experiment) showed that values (Fig. 6E) were 0.96±0.1 for cells co-expressing CFP–Bax and YFP-MFN2, and 0.9±0.1 for cells co-expressing CFP–Bax and YFP–MFN1, revealing that either MFN2 or MFN1 binds with clustering Bax with a 1:1 stoichiometry ratio.

To inspect the co-location of MFN2 or MFN1 with another pro-apoptotic Bak protein, cells were co-transfected with CFP–Bak and YFP–MFN2 or YFP–MFN1 in the presence of Z-VAD-FMK. At 14 h after transfection, cells were stained with DilC1(5) for 30 min and subsequently were imaged using our system. Fluorescence images (Fig. 7A) showed that mitochondria were not stained by DilC1(5) in cells expressing CFP–Bak, but both YFP–MFN2 and YFP–MFN1 colocalized with Bak. Interestingly, Pearson correlation analysis showed that the average R_r value (Fig. 7B) between CFP–Bak and YFP–MFN1 was 0.60±0.17, higher than the 0.39±0.16 between CFP–Bak and YFP–MFN2, implying that the relationship between MFN2 and Bak may be different from that between MFN1 and Bak.

Next, quantitative FRET measurement was further used to analyze the relationship between MFN2 and MFN1 and Bak and Mcl-1. Representative cells (Fig. 7C) co-expressing CFP–Bak and YFP–MFN1 showed higher E_D and E_A values than those for cells co-expressing CFP–Bak and YFP–MFN2. Statistical results

Journal of Cell Science (2020) 133, jcs245001. doi:10.1242/jcs.245001

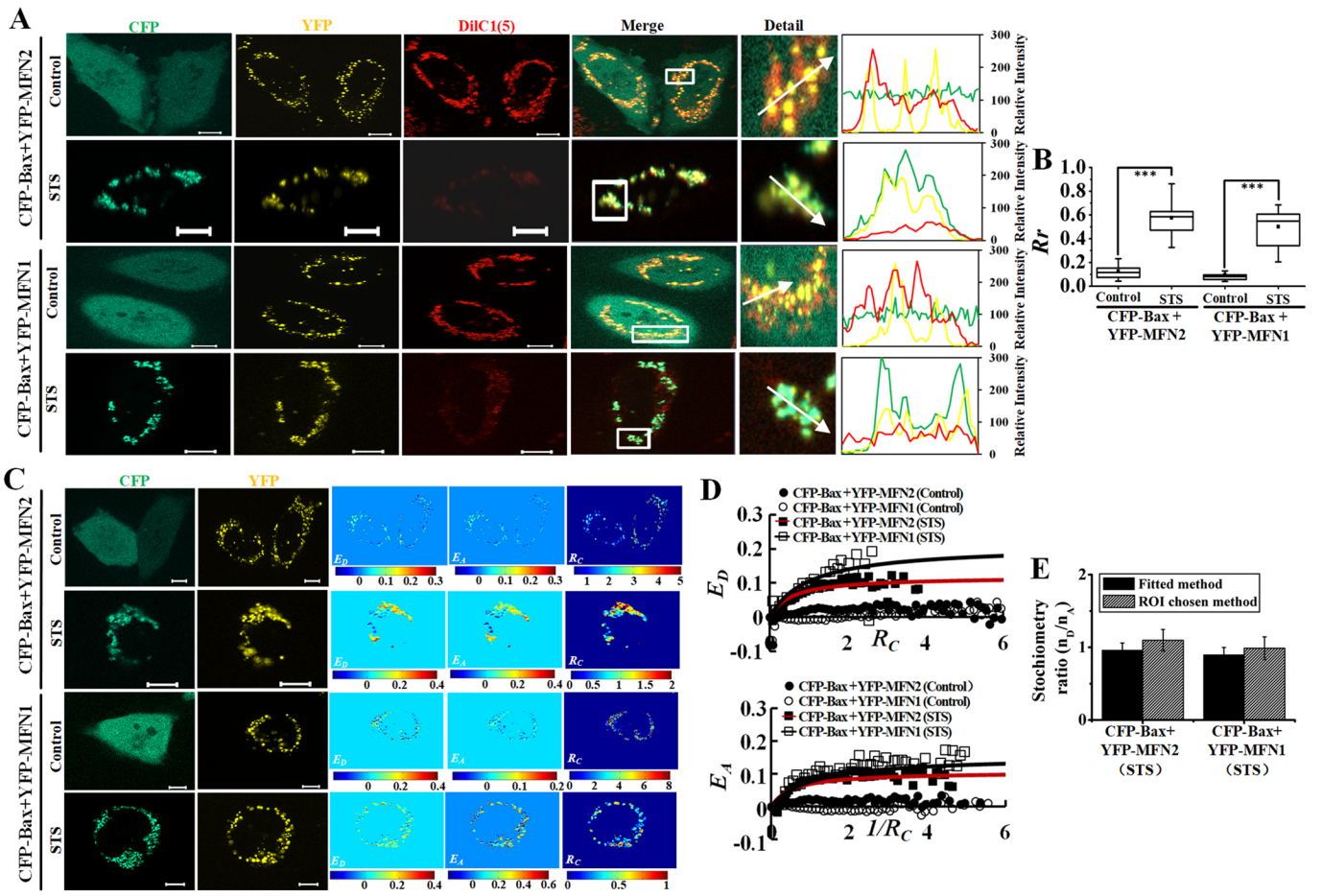

Fig. 6. MFN2 and MFN1 bind to clustered Bax but not monomeric Bax. (A) Fluorescence images of representative living or STS-treated HeLa cells co-expressing CFP–Bax and YFP–MFN2 or YFP–MFN1, and stained with DilC1(5). Detail panel shows information from white boxes in the merge images, and intensity line profiles show the fluorescence intensities of CFP, YFP and DilC1(5) along the white arrows in the merge panels. Scale bars: 10 µm. (B) R_r values for the colocalization between Bax and MFN2 or MFN1 in living or STS-treated HeLa cells expressing CFP–Bax and YFP–MFN2 or YFP–MFN1. The box represents the 25–75th percentiles, and the median is indicated by the line and the mean by a square symbol. The whiskers show the maximum and minimum values. n=20 cells. (C) Fluorescence images (DD and AA) of representative living or STS-treated cells co-expressing CFP–Bax and YFP–MFN2 or YFP–MFN1, and corresponding pixel-to-pixel pseudo-color E_D and E_A as well as R_C images. Scale bars: 10 µm. (D) E_D–R_C and E_A–$1/R_C$ plots (0.01 bin size for R_C) from living or STS-treated cells co-expressing CFP–Bax and YFP–MFN2 and YFP–MFN1 (n=62 cells each). Red lines represent the best fitted curves of data from cells co-expressing CFP–Bax+YFP–MFN2 (STS). Black lines represent fitted curves of data from cells co-expressing CFP–Bax+YFP–MFN1 (STS). (E) Stoichiometry ratio (v, n_D/n_A) of Bax to MFN2 and MFN1 in STS-treated cells from three independent experiments. Data are mean±s.d.

(Fig. 7D) (60 cells) showed that E_D or E_A values of cells co-expressing CFP–Bak and YFP–MFN2 were all lower than 0.05 in the 0–4 range of R_C or $1/R_C$, while in cells co-expressing CFP–Bak and YFP–MFN1, E_A value increased with $1/R_C$, and tended to be over 0.15 when $1/R_C$ was larger than 2. Therefore, FRET assay results also confirm that there is indeed a difference between MFN2 and MFN1, and that MFN1 but not MFN2 can bind with Bak. FRET assays also showed that MFN1 and MFN2 can bind with Mcl-1 (Fig. 7E,F).

DISCUSSION

Live-cell FRET two-hybrid assays, for the first time, demonstrate that MFN2 binds to MFN1 with 1:1 stoichiometry and both MFN2 and MFN1 can bind to Bcl-XL to form complexes with 1:1 stoichiometry. Live-cell FRET analysis also indicates that the GTPase domains of both MFN2 and MFN1 play key roles in binding with Bcl-XL. Moreover, the Bcl-XL complexed with MFN2 or MFN1 maintains its full anti-apoptotic ability. Very importantly, we also show that MFN2 but not MFN1 mediates Bcl-XL-induced mitochondrial aggregation. Bcl-XL may be an upstream factor that regulates mitochondrial dynamics by regulating the activity of both the GTPases MFN2 and MFN1.

The reason that MFN2 has a more-key role than MFN1 in Bcl-XL-induced mitochondrial aggregation may be due to the different roles of MFN2 and MFN1 in regulating mitochondrial morphology. Live-cell FRET two-hybrid assays showed that both MFN2 and MFN1 bind to Bcl-XL for forming heterotypic oligomers, which is consistent with results from previous co-IP assays (Cleland et al., 2011) in HeLa cells. However, in HEK293T cells, previous co-IP assays showed that Bcl-XL selectively co-precipitated MFN2 but not MFN1 (Delivani et al., 2006), implying different functions between MFN2 and MFN1. Indeed, a previous report showed that knocking down MFN2 induced more cells with thick fragmented mitochondria, but knocking down MFN1 induced more cells with short tubular mitochondria (Eura et al., 2003), which is consistent with our results (Fig. 4C,E). MFN2 mutant embryos have a severe disruption of the placental trophoblast giant cell layer, but MFN1-deficient giant cells are normal (Chen et al.,

Journal of Cell Science (2020) 133, jcs245001. doi:10.1242/jcs.245001

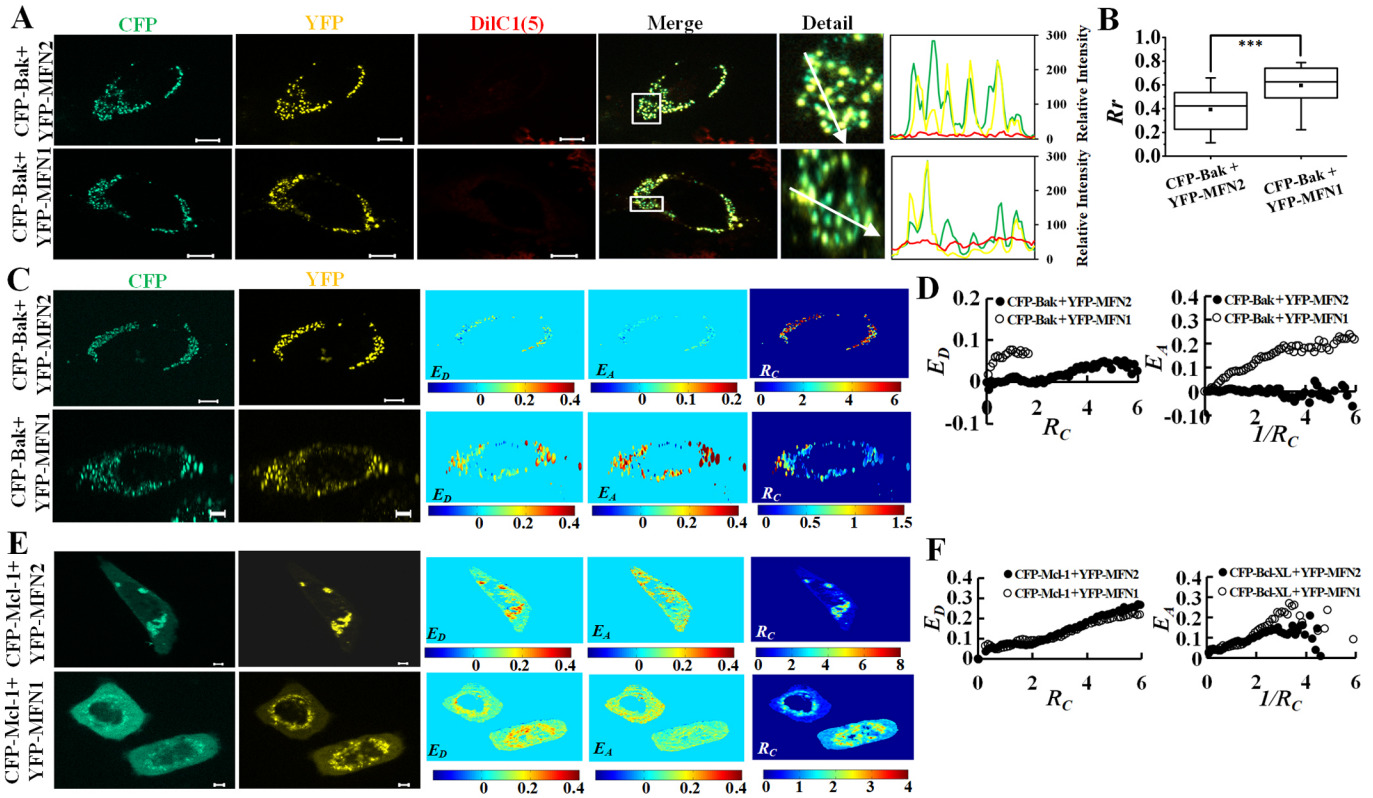

Fig. 7. FRET assay between MFN2 or MFN1 and Bak or Mcl-1. (A) Fluorescence images of representative HeLa cells co-expressing CFP–Bak and YFP–MFN2or YFP–MFN1, and stained with DilC1(5). Detail panel shows information from white boxes in the merge images, and intensity line profiles show the fluorescence intensities of CFP, YFP and DilC1(5) along the white arrows in the merge panels. Scale bars: 10 µm. (B) R_r values for the colocalization between Bak and MFN2 or MFN1 in HeLa cells expressing CFP–Bak and YFP–MFN2 or YFP–MFN1. The box represents the 25–75th percentiles, and the median is indicated by the line and the mean by a square symbol. The whiskers show the maximum and minimum values. *n*=20 cells. (C) Fluorescence images (DD and AA) of representative cells co-expressing CFP-Bak and YFP–MFN2/MFN1, and corresponding pixel-to-pixel pseudo-color E_D and E_A as well as R_C images. Scale bars: 10 µm. (D) E_D–R_C and E_A–1/R_C plots (0.01 bin size for R_C) from cells co-expressing CFP–Bak and YFP–MFN2 or YFP–MFN1 (*n*=60 cells each). (E) Fluorescence images (DD and AA) of representative cells co-expressing CFP–Mcl-1 and YFP–MFN2 or YFP–MFN1, and corresponding pixel-to-pixel pseudo-color E_D and E_A as well as R_C images. Scale bars: 10 µm. (F) E_D–R_C and E_A–1/R_C plots (0.01 bin size for R_C) from cells co-expressing CFP–Mcl-1 and YFP–MFN2 or YFP–MFN1 (*n*=60 cells each).

2003). Katsuyoshi's group also showed that MFN1 and MFN2 exhibit distinct activity in a GTP-dependent mitochondrial tethering reaction and that purified recombinant MFN1 exhibited about 8-fold higher GTPase activity than MFN2 (Ishihara et al., 2004). Recent structural studies of truncated MFN1 and MFN2 (Cao et al., 2017; Li et al., 2019) have revealed that unlike MFN1, MFN2 forms stable dimers even after GTP hydrolysis to maintain its high membrane-tethering efficiency. Our data that the values of E_D/E_A for cells co-expressing CFP–MFN2 and YFP–MFN2 were higher than those for cells co-expressing CFP–MFN1 and YFP–MFN1 (Fig. 2A) support the view that membrane-tethering efficiency of MFN2 is higher than that of MFN1. Accordingly, we propose that MFN1 plays a direct role in maintaining mitochondrial elongation, while MFN2 plays a direct role in maintaining mitochondrial tethering. Mitochondrial aggregation induced by Bcl-XL is mainly stimulated through MFN2-mediated mitochondrial tethering. Our data verify the notion that MFN2 and MFN1 play different roles in regulating mitochondrial morphology.

Our results showing that overexpression of Bcl-XL but not MFN1 or MFN2 protects against STS-induced apoptosis seems to contradict the findings that Fzo1 inhibits etoposide and anti-Fas antibody-induced apoptosis (Sugioka et al., 2004). Etoposide is in the topoisomerase inhibitor family of medication and it is believed to work by damaging DNA (Loike and Horwitz, 1976; Kalwinsky et al., 1983). Fzo1 may delay apoptosis by inhibiting apoptotic mitochondrial fission to compensate for DNA damage induced by etoposide. Mitochondrial fusion may be sufficient to delay Fas-induced apoptosis, but not enough to delay STS-induced apoptosis. It is also possible that mitochondrial fusion causes more or less delay to apoptosis, but at least in our experiment, the anti-apoptotic function of MFN2 and MFN1 is not comparable to that of Bcl-XL.

Our data also indicate that both MFN2 and MFN1 form homo-dimers to regulate mitochondrial aggregation. Analysis of the crystal structure of the HR2 domain of MFN1 resolved that HR2 polypeptide folds into a dimeric antiparallel coiled coil (Koshiba et al., 2004). Later structural and biochemical analysis revealed that the HR2 in the MFN1 may form part of the predicted helix bundle region and that membrane tethering likely needs active hydrolysis of GTP to form nucleotide-dependent dimerization of MFN1 (Qi et al., 2016). In 2017, Gao's group highlighted that dimerization of the GTPase domains of MFN1 is regulated by guanine nucleotide (Cao et al., 2017). Recently, Gao's group also proposed that MFN2 remains dimerized after GTP hydrolysis, which is in contrast to the GTP hydrolysis-dependent dimerization of MFN1 (Li et al., 2019). Here, live-cell FRET assays demonstrate the homo-oligomerization of both MFN2 and MFN1 (Fig. 2A). To further resolve the MFN2 and MFN1 homo-oligomers, we used another FRET analysis method [E_D=(1−(1/(1+R_C))^(n−1))×E_{Dmax}, where n is the number

Journal of Cell Science (2020) 133, jcs245001. doi:10.1242/jcs.245001

of homo-oligomers; see Materials and Methods] exactly as described previously (Adair and Engelman, 1994; Meyer et al., 2006) to evaluate the data in Fig. 2A, and the *n* value obtained by fitting E_D–R_C plots was 2.4 for the cells co-expressing CFP–MFN2 and YFP–MFN2, and was 2.0 for the cells co-expressing CFP–MFN1 and YFP–MFN1, indicating that both MFN2 and MFN1 regulate mitochondrial fusion, likely through forming dimers. Mitochondrial aggregation only occurs upon overexpression of MFN1, MFN2 or Bcl-XL but not lower expression levels of that. MFN-deficient cells had dramatically fragmented mitochondria, but MFN-deficient cells infected with MFN-expressing retrovirus showed predominantly tubular mitochondria (Chen et al., 2003). High levels of expression of MFN1, MFN2, Bcl-XL or incompetent MFN mutants do induce mitochondrial aggregation (Delivani et al., 2006; Sheridan et al., 2008; Eura et al., 2003). Mitochondrial aggregation may therefore occur just because there is much more MFN2 and MFN1 forming dimers. Mitochondrial aggregation may be just one step, probably one necessary step, for mitochondrial fusion. Other steps or factors, such as nucleotides, are also needed to assist mitochondrial aggregation to achieve mitochondrial fusion. The specific regulation mechanism of mitochondrial fusion or mitochondrial aggregation calls for further study.

Another question is whether Bcl-XL, mitofusins and pro-apoptotic proteins can form heterotrimers. Bcl-XL, an anti-apoptotic Bcl-2 family protein, inhibits cells apoptosis mainly through inhibiting the activation of pro-apoptotic proteins (Willis et al., 2005; Hockings et al., 2018; Ku et al., 2011). The BH1, BH2 and BH3 domains of Bcl-XL are important for heterodimerization with other pro-apoptotic proteins (Yin et al., 1994; Cheng et al., 1996; Muchmore et al., 1996; Sattler et al., 1997). Our data show that neither MFN2 nor MFN1 inhibited STS-induced cells apoptosis, but Bcl-XL complexed with MFN2 or MFN1 maintained its full anti-apoptotic ability in response to STS treatment. In other words, interaction between MFN2 or MFN1 and Bcl-XL has no significant effect on apoptosis, at least for apoptosis induced by STS. Two regulation modes can be used for explaining the full anti-apoptotic ability of the MFN2– and MFN1–Bcl-XL complex: one mode is that Bcl-XL, MFN2 and MFN1 and pro-apoptotic proteins can form heterotrimers; another mode is that association between Bcl-XL and MFN2 and MFN1 is unstable, and probably is a 'kiss-and-run'. Although a previous report showed that the chimera between Bcl-XL and Bax (Bcl-XL/Bax H5) induced substantial mitochondrial fragmentation in healthy cells via binding to MFNs (Cleland et al., 2011), it is not clear which domain of Bcl-XL plays a key role in binding with MFNs. It may be worthwhile to explore which regulation mode is dominant.

Interestingly, the GTPase domain mutants of MFN2 [MFN2(K109A)] and MFN1 [MFN1(K88T)] still had the ability to form oligomers, but lost the ability for binding with Bcl-XL. The two mutated lysine residues here belong to the conserved G2 or G1 (P-loop) motif of GTPases, which coordinate the phosphate groups of the bound guanine nucleotide (Qi et al., 2016; Cao et al., 2017; Yan et al., 2018), and the two mutants will decrease activity of GTPases (Yan et al., 2018; Ishihara et al., 2004; Detmer and Chan, 2007). In fact, we performed quantitative FRET assay for cells co-expressing CFP-labeled MFN2(K109A) and YFP-labeled MFN2(K109A), CFP-labeled MFN1(K88T) and YFP-labeled MFN1(K88T), or CFP–MFN1(K88T) and YFP–MFN2(K109A), respectively, and our results showed that MFN2(K109A) and MFN1(K88T) can form homo- and hetero-oligomers (Fig. S3), which is contrast to results from a previous report showing that MFN1(K88T)–FLAG does not co-precipitate with MFN1(K88T)–HA (Ishihara et al., 2004). However, our FRET assay demonstrated no binding between MFN2(K109A) and Bcl-XL (Fig. S4C), or between MFN1(K88T) and Bcl-XL (Fig. S4C), which is contrast to our results of co-IP assay (Fig. S4D) between CFP–Bcl-XL and MFN2(K109A)–Myc and MFN1(K88T)–Myc. One reason for this could be that different environments between living and apoptotic cells lead to different binding capacities between Bcl-XL and MFN2(K109A) or MFN1(K88T) and explain the controversial results. It is possible for that MFN2(K109A) or MFN1(K88T) binds with Bcl-XL in a kiss-and-run manner in living cells, and our FRET assay based on averages of large amounts of data will show a lower degree of such binding but that a co-IP assay would not detect this difference. These results confirm a notion that the GTPase domains of MFN2 and MFN1 play key roles in binding with Bcl-XL. Mutation of this residue would not normally affect the overall folding of the protein, but binding of the nucleotide (Yan et al., 2018). It may be worthwhile to explore whether this residue is directly involved in the interface or whether this interaction is dependent on the loading of GTP/GDP to MFNs. FRAP analysis and direct observation of fission and fusion all show that Bcl-XL overexpression significantly increases the rate of mitochondrial fusion (Berman et al., 2009; Delivani et al., 2006). Addition of purified recombinant full-length monomeric soluble Bcl-XL also stimulates mitochondrial fusion in a dose-dependent manner (Hoppins et al., 2011). *In vitro* GTPase assays performed with purified recombinant full-length Bcl-XL show that Bcl-XL increases Drp1 GTPase activity (Li et al., 2008), indicating that Bcl-XL may induce mitochondrial fragment by activating Drp1. Similar to the increased Drp1 GTPase activity mediated by Bcl-XL, Bcl-XL may increase the GTPase activity of MFN2 to induce MFN2-dependent mitochondrial aggregation.

Several studies focus on uncovering roles of Bax in regulating mitofusins to balance mitochondrial networks. The mitochondria in cells lacking Bax and Bak are shorter, have less network continuity and lower fusion rates (Karbowski et al., 2006). *In vitro* fusion assays have demonstrated that the soluble form of Bax positively regulates mitochondrial fusion exclusively through homotypic MFN2 trans complexes (Hoppins et al., 2011), and yeast two-hybrid analysis indicates that Bax selectively interacts with MFN2 and not MFN1. co-IP experiments show that Bax bound both MFN2 and MFN1 in HeLa cells (Cleland et al., 2011). In apoptotic cells, Bax and Bak colocalize with MFN2 (Karbowski et al., 2002; Youle and Karbowski, 2005), and mitochondrial fusion is blocked by the accumulation of membrane-inserted oligomerized Bax (Karbowski et al., 2004; Hoppins et al., 2011). The difference in these results may due to the experimental environment. Our live-cell FRET results show no direct binding relation between Bax and MFN2 or MFN1 in healthy cells, but both Bax–MFN2 and Bax–MFN1 complexes exist in apoptotic cells. We reason that monomeric Bax may act in two ways, by directly binding MFN2 and indirectly mediating another protein, to activate MFN2, and the second way dominates in living healthy HeLa cells. In apoptotic cells, each Bax protein in the Bax clusters can bind one MFN2 or MFN1, and oligomerized Bax seems to inhibit activation of MFN2 or MFN1 by directly binding with them.

In contrast to oligomerized Bax associating with both MFN2 and MFN1 in apoptotic cells, Bak selectively associates with MFN1 in apoptotic HeLa cells. Previous co-IP assays (Brooks et al., 2007) performed in HeLa cells show that Bak interacts with MFN1 and MFN2 in healthy HeLa cells, but Bak dissociates from MFN2 and enhances the association with MFN1 in apoptotic cells, which is consistent with our results. It is difficult to obtain cells with an R_C of

MFN1 to Bak larger than 2, which further confirms the view that only oligomerized Bak can associate with MFN1. Moreover, from E_A–$1/R_C$ and E_D–R_C plots for cells co-expressing Bak and MFN1, it can be seen that E_D or E_A values both increase with R_C or $1/R_C$, but E_A does not tend to be a constant value when $1/R_C$ was larger than 2 or even 4, probably because of multiple binding forms existing between Bak and MFN1. In addition, neither MFN2 nor MFN1 prevent apoptosis induced by oligomerized Bak (Fig. 7D) in our experiment, which is different from the results of a previous study showing that MFN2 and MFN1 expression delay Bak activation (Sugioka et al., 2004). This difference may due to overexpressed Bak having a strong ability to auto-oligomerize without apoptotic stimulus, but that MFN2 or MFN1 do not have the same ability as Bcl-XL to prevent mitochondrial Bak oligomerization (Willis et al., 2005; Hockings et al., 2018).

In summary, MFN2 and MFN1 associate with Bcl-XL to form complexes with 1:1 stoichiometry, and MFN2 but not MFN1 participates in Bcl-XL-mediated mitochondrial aggregation. In addition, the GTPase domain of MFN2 and MFN1 plays a key role in mediating binding to Bcl-XL. Neither MFN2 nor MFN1 alters the anti-apoptotic ability of Bcl-XL. These findings provide new evidence for understanding the molecular interplay between mitochondrial dynamics and apoptosis.

MATERIALS AND METHODS

DNA constructs and siRNAs

MFN2–YFP was Addgene plasmid #28010 (deposited by Richard Youle; RRID:Addgene_28010) (Karbowski et al., 2002). MFN1–Myc was Addgene plasmid #23212 (deposited by David Chan; RRID: Addgene_23212) (Chen et al., 2003). MFN2(K109A)-16xmyc was Addgene plasmid #26051 (deposited by David Chan, RRID: Addgene_26051). MFN1(K88T)-10xmyc was Addgene plasmid #26050 (also deposited by David Chan; RRID:Addgene_26050). ECFP-Bak was Addgene plasmid #31501 (deposited by Richard Youle, RRID: Addgene_31501; Nechushtan et al., 2001). pEYFP-C1-Drp1 was Addgene plasmid #45160 (deposited by Richard Youle, RRID: Addgene_45160; Frank et al., 2001). pcDNA3-CFP was Addgene plasmid #13030 (deposited by Doug Golenbock, RRID:Addgene_13030). pcDNA3-YFP was Addgene plasmid #13033 (also deposited by Doug Golenbock, RRID:Addgene_13033). CFP-Bcl-XL and CFP-Bax were kindly supplied by Andrew P. Gilmore (University of Manchester, UK; Valentijn et al., 2003). The YFP-G4-CFP (CFP–YFP dimer, C4Y) was kindly provided by Christian Wahl-Schott (Department Pharmazie, Ludwig-Maximilians-Universität München, Germany; Butz et al., 2016). mCherry-ActA (mitochondria-specific Act-A tail-anchor sequence, ActA is a control protein that does not bind to MFN2 or MFN1) was kindly provided by David W. Andrews (McMaster University, Canada; Aranovich et al., 2012). CFP–Mcl-1 plasmid was synthesized as previously described (Wang et al., 2020). To generate plasmids encoding CFP fused to MFN2, MFN1, MFN2(K109A) or MFN1(K88T) the coding region for the relevant protein was prepared by PCR from cDNA from the plasmids described above and was ligated into pECFP-C1 vector obtained by double enzyme digestion (XhoI-BamHI) of ECFP-Bak plasmid. YFP–MFN2, YFP–MFN1, YFP–MFN2(K109A) and YFP–MFN1(K88T) was generated by ligating the coding region of the relevant protein into pEYFP-C1 vector obtained by double enzyme digestion (XhoI-BamHI) of pEYFP-C1-Drp1 plasmid. CFP or YFP was fused to N-terminal of MFN2, MFN1, MFN2(K109A) or MFN1(K88T) to generate CFP-tagged MFNs or YFP-tagged MFNs, in a similar manner to that described by Brooks et al. (2007). A schematic of YFP-tagged MFNs and CFP-tagged Bcl-XL is shown in Fig. S1. We previously constructed YFP–ActA using coding region of ActA from mCherry–ActA and YFP from YFP–Bak (Yang et al., 2019).

siRNAs were used to knock down MFN2 or MFN1 in HeLa cells. The target sequences for MFN2 and MFN1 were as follows: human MFN2-siRNA, 5′-AAGGACAAGCGACACATGGCT-3′ (IGEBio, Guangzhou, China); and human MFN1-siRNA, 5′-GGCGTCCGTTACATCTAGA-3′ (RIBOBio, Guangzhou, China). Scrambled siRNAs (negative control) for MFN2-siRNA and MFN1-siRNA were purchased from IGEBio (Guangzhou, China) and RIBOBio (Guangzhou, China), respectively.

Cell culture, transfection and staining

HeLa cells obtained from the Department of Medicine (Jinan University, Guangzhou, China) were cultured exactly as described previously (Yang et al., 2019). When cells reached 70% to 90% confluence in a 30-mm glass dish, cells were transfected with the indicated amounts of DNA plasmids using TurboFect Transfection Reagent (Thermo Fisher Scientific) for 14–36 h. Fluorescence imaging was always performed after cells were transfected with Bak for 14 h but other DNA plasmids for 24 h. Cells transfected with Bak were always incubated with 10 µM of the broad-spectrum caspase inhibitor Z-VAD-FMK (Merck-Calbiochem, USA). To induce apoptosis, cells transfected with the indicated plasmids were treated with 2 µM staurosporine (STS) (Sigma, Santa Clara, USA), an apoptotic-positive drug, for 5 h.

For transfection of siRNAs, cells at 30% to 50% confluence were transfected with 50 nM of siRNA by using Lipofectamine 2000 (Invitrogen, Carlsbad, USA) for 48 h, and then subjected to western blot analysis. For cells that needed to be transfected with both siRNA and DNA plasmids, cells were first transfected with siRNAs and then transfected with DNA plasmids on the next day.

To visualize mitochondrial morphology, the transfected cells were incubated with 50 nM DilC1(5) (Invitrogen, Carlsbad, USA), or 250 nM MitoTracker Deep Red 633 dye (Invitrogen, Carlsbad, USA) for 30 min, and then washed twice with PBS before imaging. Hoechst 33258 (Gclone, #CS2307) was used for staining nuclear DNA.

Antibodies

Primary antibodies were used in this study as follows: anti-MFN2 rabbit monoclonal antibody (11925S, Cell Signaling Technology), anti-MFN1 rabbit monoclonal antibody (14739S, Cell Signaling Technology), anti-Myc-tag mouse monoclonal antibody (2276S, Cell Signaling Technology), anti-GFP mouse monoclonal antibody (HT801, TransGen Biotech) and anti-GAPDH mouse mAb(2B8) (TDY042, TDY Biotech). Because CFP and GFP are both labeled by the same primary anti-GFP antibody, anti-GFP antibody was used for anti-CFP in this report. Primary antibodies were used at 1:1000 overnight at 4°C. Secondary antibodies used for western blotting include: Alexa Fluor® 790 AffiniPure goat anti-rabbit IgG (H+L) (1:20,000; 111655144, Jackson ImmunoResearch) and HRP affinipure goat anti-mouse IgG (H+L) (1:10,000; S001, TDY Biotech). Antibodies were used according to the manufacturer's recommendations. GAPDH was used as loading control. Anti-Myc-tag mouse monoclonal antibody (1:1000) was also used for the immunoprecipitation assay.

Western blotting and immunoprecipitation assays were performed as described previously (Wang et al., 2019; Yu et al., 2020).

Microscopy imaging

Microscopy imaging was performed on a Zeiss ApoTome.2 image system (Axio Observer 7, Carl Zeiss, Oberkochen, Germany) equipped with an inverted wide-field fluorescence microscope, an ApoTome.2 module for structured illumination and a CCD camera for imaging (Axiocam 506 mono, Carl Zeiss, Oberkochen, Germany). The wide-field fluorescence microscope consists of a metal halide lamp (X-Cite 120, 120Q, Excelitas, MA, USA), a 63×1.4 NA oil immersion and five filter-cubes. A cube comprising a BP436/20 excitation filter (Carl Zeiss, Germany) and a dichroic mirror of DFT 455 (Carl Zeiss, Germany) as well as a BP480/40 emission filter (Carl Zeiss, Germany) was used for donor imaging (I_{DD}); a cube comprising a BP500/20 excitation filter (Carl Zeiss, Germany) and a dichroic mirror of DFT 515 (Carl Zeiss, Germany) as well as a BP535/30 emission filter (Carl Zeiss, Germany) was used for acceptor imaging (I_{AA}); a cube comprising a BP436/20 excitation filter (Carl Zeiss, Germany) and a dichroic mirror of DFT 455 (Carl Zeiss, Germany) as well as a BP535/30 emission filter (Carl Zeiss, Germany) was used for FRET imaging (I_{DA}). A cube comprising a BP565/30 nm excitation filter (Carl Zeiss, Germany) and

a dichroic mirror of FT585 (Carl Zeiss, Germany) as well as a BP620/60 nm emission filter (Carl Zeiss, Germany) was used for imaging Mito-Tracker Deep Red 633 and DiIC1(5). A cube comprising a BP359/48 nm excitation filter (Carl Zeiss, Germany) and a dichroic mirror of FT395 (Carl Zeiss, Germany) as well as a BP445/50 nm emission filter (Carl Zeiss, Germany) was used for imaging Hoechst 33258.

FRET two-hybrid assay

Measurement of FRET efficiency and total concentration ratio of acceptor to donor molecules

Donor-centric FRET efficiency (E_D) and acceptor-centric FRET efficiency (E_A), as well as the total concentration ratio (R_C) of acceptor to donor molecules, were determined as follows (Butz et al., 2016; Erickson et al., 2001; Hoppe et al., 2002; Zal and Gascoigne, 2004; Chen et al., 2006):

$$E_D = \frac{F_C}{F_C + GI_{DD}}, \quad (1)$$

$$E_A = \frac{F_C}{aI_{AA}} \frac{\varepsilon_A(\lambda_D)}{\varepsilon_D(\lambda_D)}, \quad (2)$$

$$R_C = \frac{kI_{AA}}{F_C/G + I_{DD}}, \quad (3)$$

where

$$F_C = I_{DA} - a(I_{AA} - cI_{DD}) - d(I_{DD} - bI_{AA}). \quad (4)$$

$\varepsilon_A(\lambda_D)$ and $\varepsilon_D(\lambda_D)$ are the absorption coefficient of acceptor (A) and donor (D) at donor excitation the wavelength (λ_D), respectively; F_C is sensitized emission fluorescence; a and b are acceptor bleedthrough in the I_{DA} and I_{DD} filter sets, and c and d are donor bleedthrough in the I_{AA} and I_{DA} filter sets, respectively. G is the ratio of the sensitized emission of acceptor to an equivalent quenching of donor and k is the ratio of donor-to-acceptor fluorescence intensity for equimolar concentrations in the absence of FRET. G, k and $\varepsilon_A/\varepsilon_D$ can be predetermined using a tandem CFP–YFP dimer as described previously (Du et al., 2018).

Obtaining maximum FRET efficiency

To obtain E_{Dmax} (maximum E_D, the E_D when all donor molecules are bound to acceptor) and the saturation binding curve of E_D to R_C, E_D values were distributed into bins according to R_C and plotted against R_C with the function as follows (Aranovich et al., 2012; Zacharias et al., 2002):

$$E_D = \frac{E_{Dmax}R_C}{K_d + R_C}, \quad (5)$$

where K_d is the relative equilibrium dissociation constant. Similar arguments can be used to show the relationship between E_A and $1/R_C$ as follows:

$$E_A = \frac{E_{Amax}(1/R_C)}{K_d + (1/R_C)}, \quad (6)$$

where E_{Amax} is the maximum E_A when all acceptor molecules are bound to donor. According to Eqns 5 and 6, E_{Amax} and E_{Dmax} can be determined by simultaneously fitting E_D–R_C and E_A–$1/R_C$ plots.

Determination of stoichiometry

The stoichiometry (v) of a D–A complex is determined by using the E_{Dmax} and E_{Amax} values as follows (Ben-Johny et al., 2016):

$$v = \frac{n_D}{n_A} = \frac{E_{Amax}}{E_{Dmax}}, \quad (7)$$

where n_X is the number of X molecules in the D-A complex.

Statistics

Image analysis was conducted with ZEN 2.3 software (Carl Zeiss, Oberkochen, Germany) and Image-Pro Plus (Media Cybernetics, Maryland, USA). Statistical and graphical analyses were done using the software SPSS 22 (SPSS, Chicago, USA) and Origin 8.0 (OriginLab, Massachusetts, USA).

Acknowledgements

We would like to thank Dr Andrew P. Gilmore for providing CFP-BCL-XL and CFP-Bax plasmids, and Christian Wahl-Schott for providing YFP-G4-CFP plasmid.

Competing interests

The authors declare no competing or financial interests.

Author contributions

Conceptualization: M.D., T.C.; Methodology: M.D., S.Y., W.S., X.W.; Software: M.D., W.S., F.Y., Y.L., Y.W.; Validation: M.D., M.Z., Y.L., Z.M.; Formal analysis: M.D., S.Y., W.S., Y.W.; Investigation: M.D., M.Z., Y.L., Z.M., X.W.; Resources: M.D., S.Y., F.Y.; Data curation: M.D., S.Y., W.S., M.Z., F.Y., Y.L., Z.M., Y.W.; Writing - original draft: M.D., T.C.; Writing - review & editing: M.D., T.C.; Visualization: M.D., S.Y., W.S., M.Z., F.Y., X.W.; Supervision: M.D., X.W., T.C.; Project administration: M.D., X.W., T.C.; Funding acquisition: T.C.

Funding

This work was supported by the National Natural Science Foundation of China (grant numbers 61527825 and 61875056), and Science and Technology Program of Guangzhou (grant number 2019050001).

Supplementary information

Supplementary information available online at
https://jcs.biologists.org/lookup/doi/10.1242/jcs.245001.supplemental

Peer review history

The peer review history is available online at
https://jcs.biologists.org/lookup/doi/10.1242/jcs.245001.reviewer-comments.pdf

References

Adair, B. D. and Engelman, D. M. (1994). Glycophorin A helical transmembrane domains dimerize in phospholipid bilayers: a resonance energy transfer study. *Biochemistry* **33**, 5539-5544. doi:10.1021/bi00184a024

Aranovich, A., Liu, Q., Collins, T., Geng, F., Dixit, S., Leber, B. and Andrews, D. W. (2012). Differences in the mechanisms of proapoptotic BH3 proteins binding to Bcl-XL and Bcl-2 quantified in live MCF-7 cells. *Mol. Cell* **45**, 754-763. doi:10.1016/j.molcel.2012.01.030

Ben-Johny, M., Yue, D. N. and Yue, D. T. (2016). Detecting stoichiometry of macromolecular complexes in live cells using FRET. *Nat. Commun.* **7**, 1-10. doi:10.1038/ncomms13709

Berman, S. B., Chen, Y.-B., Qi, B., McCaffery, J. M., Rucker, E. B., Goebbels, S., Nave, K.-A., Arnold, K. A. Jonas, E. A., Pineda, F. J. et al. (2009). Bcl-xl increases mitochondrial fission, fusion, and biomass in neurons. *J. Cell Biol.* **184**, 707-719. doi:10.1083/jcb.200809060

Breckenridge, D. G., Stojanovic, M., Marcellus, R. C. and Shore, G. C. (2003). Caspase cleavage product of BAP31 induces mitochondrial fission through endoplasmic reticulum calcium signals, enhancing cytochrome c release to the cytosol. *J. Cell Biol.* **160**, 1115-1127. doi:10.1083/jcb.200212059

Brookes, P. S., Yoon, Y., Robotham, J. L., Anders, M. W. and Sheu, S.-S. (2004). Calcium, ATP, and ROS: a mitochondrial love-hate triangle. *Am. J. Physiol. Cell Physiol.* **287**, C817-C833. doi:10.1152/ajpcell.00139.2004

Brooks, C., Wei, Q., Feng, L., Dong, G., Tao, Y., Mei, L., Xie, Z.-J. and Dong, Z. (2007). Bak regulates mitochondrial morphology and pathology during apoptosis by interacting with mitofusins. *Proc. Natl. Acad. Sci. USA* **104**, 11649-11654. doi:10.1073/pnas.0703976104

Butz, E. S., Ben-Johny, M., Shen, M., Yang, P. S., Sang, L., Biel, M., Yue, D. T. and Wahl-Schott, C. (2016). Quantifying macromolecular interactions in living cells using FRET two-hybrid assays. *Nat. Protoc.* **11**, 2470-2498. doi:10.1038/nprot.2016.128

Cao, Y.-L., Meng, S., Chen, Y., Feng, J.-X., Gu, D.-D., Yu, B., Li, Y.-J., Yang, J.-Y., Liao, S., Chan, D. C. et al. (2017). MFN1 structures reveal nucleotide-triggered dimerization critical for mitochondrial fusion. *Nature* **542**, 372-376. doi:10.1038/nature21077

Chen, H., Detmer, S. A., Ewald, A. J., Griffin, E. E., Fraser, S. E. and Chan, D. C. (2003). Mitofusins Mfn1 and Mfn2 coordinately regulate mitochondrial fusion and are essential for embryonic development. *J. Cell Biol.* **160**, 189-200. doi:10.1083/jcb.200211046

Chen, H., Puhl, H. L., III, Koushik, S. V., Vogel, S. S. and Ikeda, S. R. (2006). Measurement of FRET efficiency and ratio of donor to acceptor concentration in living cells. *Biophys. J.* **91**, L39-L41. doi:10.1529/biophysj.106.088773

Chen, H.-C., Kanai, M., Inoue-Yamauchi, A., Tu, H.-C., Huang, Y., Ren, D., Kim, H., Takeda, S., Reyna, D. E., Chan, P. M. et al. (2015). An interconnected

hierarchical model of cell death regulation by the BCL-2 family. *Nat. Cell Biol.* **17**, 1270-1281. doi:10.1038/ncb3236

Cheng, E. H. Y., Levine, B. and Boise, L. H. (1996). Thompson CB and Hardwick JM. Bax independent inhibition of apoptosis by Bcl-X(L). *Nature* **379**, 554-556. doi:10.1038/379554a0

Cleland, M. M., Norris, K. L., Karbowski, M., Wang, C., Suen, D.-F., Jiao, S., George, N. M., Luo, X., Li, Z. and Youle, R. J. (2011). Bcl-2 family interaction with the mitochondrial morphogenesis machinery. *Cell Death Differ.* **18**, 235-247. doi:10.1038/cdd.2010.89

Delivani, P., Adrain, C., Taylor, R. C., Duriez, P. J. and Martin, S. J. (2006). Role for CED-9 and Egl-1 as regulators of mitochondrial fission and fusion dynamics. *Mol. Cell* **21**, 761-773. doi:10.1016/j.molcel.2006.01.034

Detmer, S. A. and Chan, D. C. (2007). Complementation between mouse Mfn1 and Mfn2 protects mitochondrial fusion defects caused by CMT2A disease mutations. *J. Cell Biol.* **176**, 405-414. doi:10.1083/jcb.200611080

Du, M., Yang, F., Mai, Z., Qu, W., Lin, F., Wei, L. and Chen, T. (2018). FRET two-hybrid assay by linearly fitting FRET efficiency to concentration ratio between acceptor and donor. *Appl. Phys. Lett.* **112**, 153702. doi:10.1063/1.5021466

Erickson, M. G., Alseikhan, B. A., Peterson, B. Z. and Yue, D. T. (2001). Preassociation of calmodulin with voltage-gated Ca^{2+} channels revealed by FRET in single living cells. *Neuron* **31**, 973-985. doi:10.1016/S0896-6273(01)00438-X

Eura, Y., Ishihara, N., Yokota, S. and Mihara, K. (2003). Two mitofusin proteins, mammalian homologues of FZO, with distinct functions are both required for mitochondrial fusion. *J. Biochem.* **134**, 333-344. doi:10.1093/jb/mvg150

Fannjiang, Y., Cheng, W. C., Lee, S. J., Qi, B., Pevsner, J., McCaffery, J. M., Hill, R. B. and Basañez, G. (2004). Mitochondrial fission proteins regulate programmed cell death in yeast. *Gene. Dev.* **18**, 2785-2797. doi:10.1101/gad.1247904

Frank, S., Gaume, B., Bergmann-Leitner, E. S., Leitner, W. W., Robert, E. G., Catez, F., Smith, C. L. and Youle, R. J. (2001). The role of dynamin-related protein 1, a mediator of mitochondrial fission, in apoptosis. *Dev. Cell.* **1**, 515-525. doi:10.1016/S1534-5807(01)00055-7

Gandre-Babbe, S. and van der Bliek, A. M. (2008). The novel tail-anchored membrane protein Mff controls mitochondrial and peroxisomal fission in mammalian cells. *Mol. Biol. Cell* **19**, 2402-2412. doi:10.1091/mbc.e07-12-1287

Goyal, G., Fell, B., Sarin, A., Youle, R. J. and Sriram, V. (2007). Role of mitochondrial remodeling in programmed cell death in Drosophila melanogaster. *Dev. Cell* **12**, 807-816. doi:10.1016/j.devcel.2007.02.002

Gross, A. and Katz, S. G. (2017). Non-apoptotic functions of BCL-2 family proteins. *Cell Death Differ.* **24**, 1348-1358. doi:10.1038/cdd.2017.22

Hockings, C., Alsop, A. E., Fennell, S. C., Lee, E. F., Fairlie, W. D., Dewson, G. and Kluck, R. M. (2018). Mcl-1 and Bcl-xL sequestration of Bak confers differential resistance to BH3-only proteins. *Cell Death Differ.* **25**, 721-734. doi:10.1038/s41418-017-0010-6

Hoppe, A., Christensen, K. and Swanson, J. A. (2002). Fluorescence resonance energy transfer-based stoichiometry in living cells. *Biophys. J.* **83**, 3652-3664. doi:10.1016/S0006-3495(02)75365-4

Hoppins, S., Edlich, F., Cleland, M. M., Banerjee, S., McCaffery, J. M., Youle, R. J. and Nunnari, J. (2011). The soluble form of Bax regulates mitochondrial fusion via MFN2 homotypic complexes. *Mol. Biol.* **41**, 150-160. doi:10.1016/j.molcel.2010.11.030

Ishihara, N., Eura, Y. and Mihara, K. (2004). Mitofusin 1 and 2 play distinct roles in mitochondrial fusion reactions via GTPase activity. *J. Cell Sci.* **117**, 6535-6546. doi:10.1242/jcs.01565

Ishihara, N., Fujita, Y., Oka, T. and Mihara, K. (2006). Regulation of mitochondrial morphology through proteolytic cleavage of OPA1. *EMBO J.* **25**, 2966-2977. doi:10.1038/sj.emboj.7601184

Jagasia, R., Grote, P., Westermann, B. and Conradt, B. (2005). DRP-1-mediated mitochondrial fragmentation during EGL-1-induced cell death in C. elegans. *Nature* **433**, 754-760. doi:10.1038/nature03316

James, D. I., Parone, P. A., Mattenberger, Y. and Martinou, J.-C. (2003). hFis1, a novel component of the mammalian mitochondrial fission machinery. *J. Biol. Chem.* **278**, 36373-36379. doi:10.1074/jbc.M303758200

Kalwinsky, D. K., Look, A. T., Ducore, J. and Fridland, A. (1983) Effects of the epipodophyllotoxin VP-16-213 on cell cycle traverse, DNA synthesis, and DNA strand size in cultures of human leukemic lymphoblasts. *Cancer Res.* **43**, 1592-1597.

Karbowski, M., Lee, Y.-J., Gaume, B., Jeong, S.-Y., Frank, S., Nechushtan, A., Santel, A., Fuller, M., Smith, C. L. and Youle, R. J. (2002). Spatial and temporal association of Bax with mitochondrial fission sites, Drp1, and Mfn2 during apoptosis. *J. Cell Biol.* **159**, 931-938. doi:10.1083/jcb.200209124

Karbowski, M., Arnoult, D., Chen, H., Chan, D. C., Smith, C. L. and Youle, R. J. (2004). Quantitation of mitochondrial dynamics by photolabeling of individual organelles shows that mitochondrial fusion is blocked during the Bax activation phase of apoptosis. *J. Cell Biol.* **164**, 493-499. doi:10.1083/jcb.200309082

Karbowski, M., Norris, K. L., Cleland, M. M., Jeong, S.-Y. and Youle, R. J. (2006). Role of Bax and Bak in mitochondrial morphogenesis. *Nature* **443**, 658. doi:10.1038/nature05111

Koshiba, T., Detmer, S. A., Kaiser, J. T., Chen, H., McCaffery, J. M. and Chan, D. C. (2004). Structural basis of mitochondrial tethering by mitofusin complexes. *Science* **305**, 858-862. doi:10.1126/science.1099793

Ku, B., Liang, C., Jung, J. U. and Oh, B.-H. (2011). Evidence that inhibition of BAX activation by BCL-2 involves its tight and preferential interaction with the BH3 domain of BAX. *Cell Res.* **21**, 627-641. doi:10.1038/cr.2010.149

Labbé, K., Murley, A. and Nunnari, J. (2014). Determinants and functions of mitochondrial behavior. *Ann. Rev. Cell Dev. Biol.* **30**, 357-391. doi:10.1146/annurev-cellbio-101011-155756

Legros, F., Lombès, A., Frachon, P. and Rojo, M. (2002). Mitochondrial fusion in human cells is efficient, requires the inner membrane potential, and is mediated by mitofusins. *Mol. Biol. Cell* **13**, 4343-4354. doi:10.1091/mbc.e02-06-0330

Li, H., Chen, Y., Jones, A. F., Sanger, R. H., Collis, L. P., Flannery, R., McNay, E. C., Yu, T., Schwarzenbacher, R., Bossy, B. et al. (2008). Bcl-xL induces Drp1-dependent synapse formation in cultured hippocampal neurons. *Proc. Natl. Acad. Sci. USA* **105**, 2169-2174. doi:10.1073/pnas.0711647105

Li, Y. J., Cao, Y. L., Feng, J. X., Qi, Y., Meng, S., Yang, J. F., Zhong, Y. T., Kang, S., Chen, X., Lan, L. et al. (2019). Structural insights of human mitofusin-2 into mitochondrial fusion and CMT2A onset. *Nat. Commun.* **10**, 1-14. doi:10.1038/s41467-018-07882-8

Loike, J. D. and Horwitz, S. B. (1976) Effect of VP-16-213 on the intracellular degradation of DNA in HeLa cells. *Biochemistry* **15**, 5443-5448. doi:10.1021/bi00670a004

Meeusen, S., McCaffery, J. M. and Nunnari, J. (2004). Mitochondrial fusion intermediates revealed in vitro. *Science* **305**, 1747-1752. doi:10.1126/science.1100612

Meyer, B. H., Segura, J.-M., Martinez, K. L., Hovius, R., George, N., Johnsson, K. and Vogel, H. (2006). FRET imaging reveals that functional neurokinin-1 receptors are monomeric and reside in membrane microdomains of live cells. *Proc. Natl Acad. Sci. USA* **103**, 2138-2143. doi:10.1073/pnas.0507686103

Muchmore, S. W., Sattler, M., Liang, H., Meadows, R. P., Harlan, J. E., Yoon, H. S., Nettesheim, D., Chang, B. S., Thompson, C. B., Wong, S.-L. et al. (1996). X-ray and NMR structure of human Bcl-xL, an inhibitor of programmed cell death. *Nature* **381**, 335-341. doi:10.1038/381335a0

Nakada, K., Inoue, K., Ono, T., Isobe, K., Ogura, A., Goto, Y.-I., Nonaka, I. and Hayashi, J.-I. (2001). Inter-mitochondrial complementation: mitochondria-specific system preventing mice from expression of disease phenotypes by mutant mtDNA. *Nat. Med.* **7**, 934-940. doi:10.1038/90976

Nechushtan, A., Smith, C. L., Lamensdorf, I., Yoon, S.-H. and Youle, R. J. (2001). Bax and Bak coalesce into novel mitochondria-associated clusters during apoptosis. *J. Cell Biol.* **153**, 1265-1276. doi:10.1083/jcb.153.6.1265

Neuspiel, M., Zunino, R., Gangaraju, S., Rippstein, P. and McBride, H. H. (2005). Activated mitofusin 2 signals mitochondrial fusion, interferes with Bax activation, and reduces susceptibility to radical induced depolarization. *J. Biol. Chem.* **280**, 25060-25070. doi:10.1074/jbc.M501599200

Olichon, A., Baricault, L., Gas, N., Guillou, E., Valette, A., Belenguer, P. and Lenaers, G. (2002). Loss of OPA1 perturbates the mitochondrial inner membrane structure and integrity, leading to cytochrome c release and apoptosis. *J. Biol. Chem.* **278**, 7743-7746. doi:10.1074/jbc.C200677200

Palmer, C. S., Osellame, L. D., Laine, D., Koutsopoulos, O. S., Frazier, A. E. and Ryan, M. T. (2011). MiD49 and MiD51, new components of the mitochondrial fission machinery. *EMBO Rep.* **12**, 565-573. doi:10.1038/embor.2011.54

Pinton, P., Ferrari, D., Rapizzi, E., Di Virgilio, F., Pozzan, T. and Rizzuto, R. (2001). The Ca^{2+} concentration of the endoplasmic reticulum is a key determinant of ceramide–induced apoptosis: significance for the molecular mechanism of Bcl–2 action. *EMBO J.* **20**, 2690-2701. doi:10.1093/emboj/20.11.2690

Qi, Y., Yan, L., Yu, C., Guo, X., Zhou, X., Hu, X., Huang, X., Rao, Z., Lou, Z. and Hu, J. (2016). Structures of human mitofusin 1 provide insight into mitochondrial tethering. *J. Cell Biol.* **215**, 621-629. doi:10.1083/jcb.201609019

Santel, A. and Fuller, M. T. (2001). Control of mitochondrial morphology by a human mitofusin. *J. Cell Sci.* **114**, 867-874.

Sattler, M., Liang, H., Nettesheim, D., Meadows, R. P., Harlan, J. E., Eberstadt, M., Yoon, H. S., Shuker, S. B., Chang, B. S., Minn, A. J. et al. (1997). Structure of Bcl-xL-Bak peptide complex: recognition between regulators of apoptosis. *Science* **275**, 983-986. doi:10.1126/science.275.5302.983

Sheridan, C., Delivani, P., Cullen, S. P. and Martin, S. J. (2008). Bax-or Bak-induced mitochondrial fission can be uncoupled from cytochrome C release. *Mol. Cell* **31**, 570-585. doi:10.1016/j.molcel.2008.08.002

Smirnova, E., Griparic, L., Shurland, D.-L. and van der Bliek, A. M. (2001). Dynamin-related protein Drp1 is required for mitochondrial division in mammalian cells. *Mol. Biol. Cell* **12**, 2245-2256. doi:10.1091/mbc.12.8.2245

Sugioka, R., Shimizu, S. and Tsujimoto, Y. (2004). Fzo1, a protein involved in mitochondrial fusion, inhibits apoptosis. *J. Biol. Chem.* **279**, 52726-52734. doi:10.1074/jbc.M408910200

Valentijn, A. J., Metcalfe, A. D., Kott, J., Streuli, C. H. and Gilmore, A. P. (2003). Spatial and temporal changes in Bax subcellular localization during anoikis. *J. Cell Biol.* **162**, 599-612. doi:10.1083/jcb.200302154

Wallace, D. C. (2005). A mitochondrial paradigm of metabolic and degenerative diseases, aging, and cancer: a dawn for evolutionary medicine. *Annu. Rev. Genet.* **39**, 359-407. doi:10.1146/annurev.genet.39.110304.095751

Wang, C. and Youle, R. J. (2009). The role of mitochondria in apoptosis. *Annu. Rev. Genet.* **43**, 95-118. doi:10.1146/annurev-genet-102108-134850

Wang, L., Mai, Z., Zhao, M., Wang, B., Yu, S., Wang, X. and Chen, T. (2019). Aspirin induces oncosis in tumor cells. *Apoptosis* **24**, 758-772. doi:10.1007/s10495-019-01555-7

Wang, Y., Su, W. H., Mai, Z. H., Yu, S. and Chen, T. S. (2020). Anti-apoptotic capacity of mcl-1Δ127. *Biochem. Biophys. Res. Commun.* **526**, 1042-1048. doi:10.1016/j.bbrc.2020.03.181

Willis, S. N., Chen, L., Dewson, G., Wei, A., Naik, E., Fletcher, J. I., Adams, J. M. and Huang, D. C. (2005). Proapoptotic Bak is sequestered by Mcl-1 and Bcl-xL, but not Bcl-2, until displaced by BH3-only proteins. *Gene. Dev.* **19**, 1294-1305. doi:10.1101/gad.1304105

Yan, L., Qi, Y., Huang, X., Yu, C., Lan, L., Guo, X., Rao, Z., Hu, J. and Lou, Z. (2018). Structural basis for GTP hydrolysis and conformational change of MFN1 in mediating membrane fusion. *Nat. Struct. Mol. Biol.* **25**, 233-243. doi:10.1038/s41594-018-0034-8

Yang, F., Qu, W., Du, M., Mai, Z., Wang, B., Ma, Y., Wang, X. and Chen, T. (2019). Stoichiometry and regulation network of Bcl-2 family complexes quantified by live-cell FRET assay. *Cell. Mol. Life Sci.* **77**, 2387-2406. doi:10.1007/s00018-019-03286-z

Yin, X. M., Oltval, Z. M. and Korsmeyer, S. J. (1994). BH1 and BH2 domains of Bcl-2 are required for inhibition of apoptosis and heterodimerization with Bax. *Nature* **369**, 321-323. doi:10.1038/369321a0

Youle, R. J. and Karbowski, M. (2005). Mitochondrial fission in apoptosis. *Nat. Rev. Mol. Cell Biol.* **6**, 657-663. doi:10.1038/nrm1697

Yu, S., Du, M., Yin, A., Mai, Z., Wang, Y., Zhao, M., Wang, X. and Chen, T. (2020). Bcl-xL inhibits PINK1/Parkin-dependent mitophagy by preventing mitochondrial Parkin accumulation. *Int. J. Biochem. Cell Biol.* **122**, 105720. doi:10.1016/j.biocel.2020.105720

Zacharias, D. A., Violin, J. D., Newton, A. C. and Tsien, R. Y. (2002). Partitioning of lipid-modified monomeric GFPs into membrane microdomains of live cells. *Science* **296**, 913-916. doi:10.1126/science.1068539

Zal, T. and Gascoigne, N. R. J. (2004). Photobleaching-corrected FRET efficiency imaging of live cells. *Biophys. J.* **86**, 3923-3939. doi:10.1529/biophysj.103.022087

Zhu, W., Cowie, A., Wasfy, G. W., Penn, L. Z., Leber, B. and Andrews, D. W. (1996) Bcl-2 mutants with restricted subcellular location reveal spatially distinct pathways for apoptosis in different cell types. *EMBO J.* **15**, 4130-4141. doi:10.1002/j.1460-2075.1996.tb00788.x

Züchner, S., Mersiyanova, I. V., Muglia, M., Bissar-Tadmouri, N., Rochelle, J., Dadali, E. L., Zappia, M., Nelis, E., Patitucci, A., Senderek, J. et al. (2004). Mutations in the mitochondrial GTPase mitofusin 2 cause Charcot–Marie–Tooth neuropathy type 2A. *Nat. Genet.* **36**, 449-451. doi:10.1038/ng1341

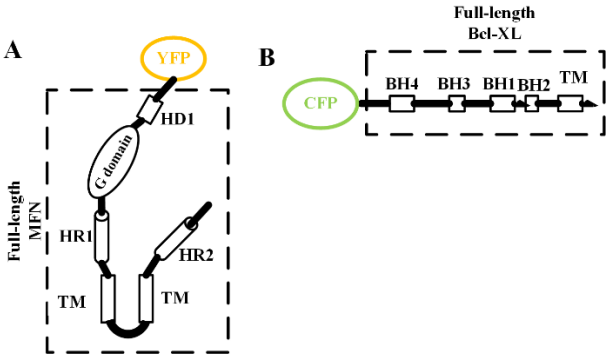

Fig. S1 Schematic to YFP-MFN (A) and CFP-Bcl-XL(B). HD1, helical domain 1; G domain, GTPase domain; HR1, heptad repeat region 1; HR2, heptad repeat region 2; TM, transmembrane region. BH, conserved Bcl-2 homology domains.

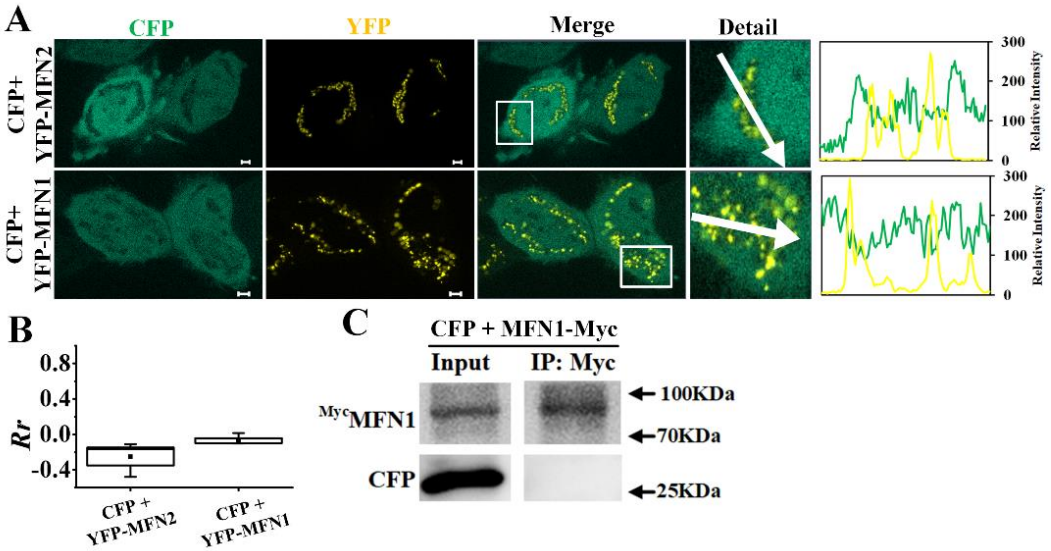

Fig. S2 CFP cannot bind to MFN2/MFN1. A Fluorescence images of representative living Hela cells co-expressing CFP and YFP-MFN2/YFP-MFN1. Detail panels show information of the white boxes in the merge images, and intensity line profiles show the fluorescence intensities of CFP and YFP- along the selected white arrow lines in the merge panels. Scale bar: 10 μm. B Statistical R_r values for the colocalization between CFP and YFP- in cells co-expressing CFP and YFP-MFN2/YFP-MFN1. n ≥ 20 cells each. C Co-immunoprecipitation assay between CFP and MFN1. Lysates prepared from Hela cells co-transfected with CFP and MFN1-Myc for 24 h subjected to immunoprecipitation with anti-Myc antibody, followed by anti-Myc and anti-CFP immunoblotting.

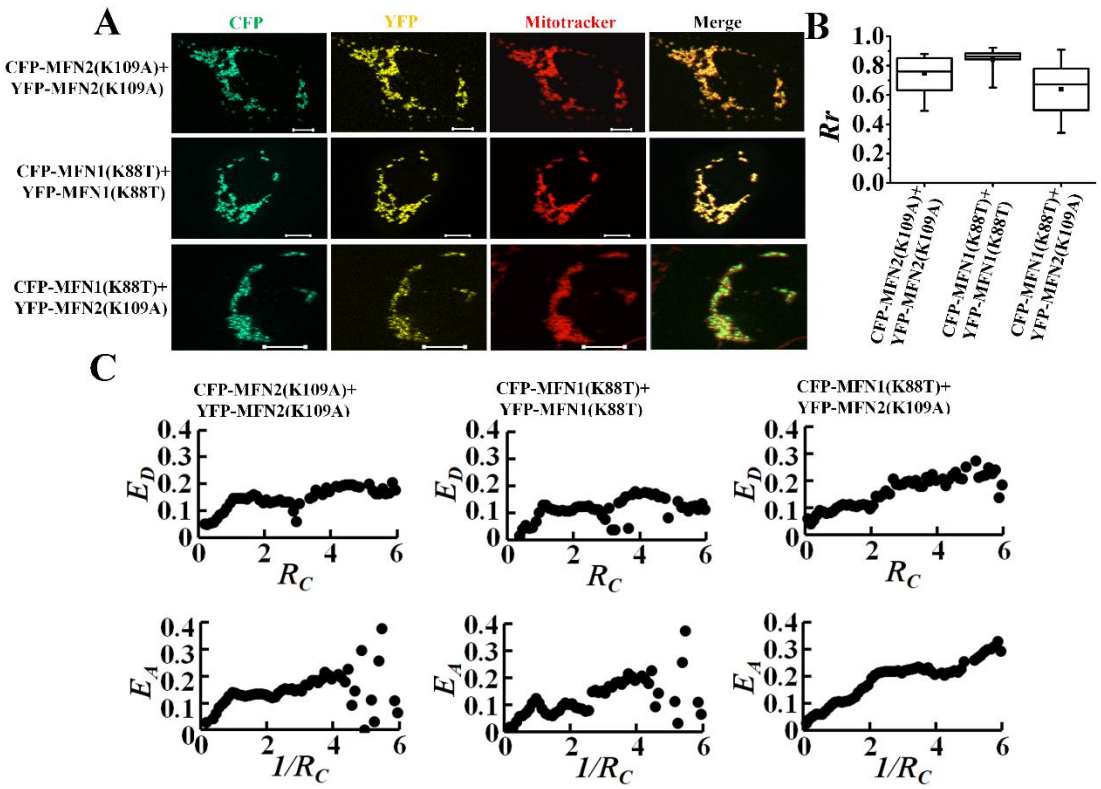

Fig. S3. Homo-/hetero-oligomerization of GTPase domain mutants of MFN2 (MFN2(K109A)) and MFN1 (MFN1(K88T)). A Fluorescence images of representative living Hela cells co-expressing CFP-MFN2(K109A) + YFP-MFN2(K109A), CFP-MFN1(K88T) + YFP-MFN1(K88T), CFP-MFN1(K88T) + YFP-MFN2(K109A), and the corresponding merge images. B Statistical R_r values for the colocalization between CFP-MFN2(K109A) and YFP-MFN2(K109A), between CFP-MFN1(K88T) and YFP-MFN1(K88T), and between CFP-MFN1(K88T) and YFP-MFN2(K109A). n ≥ 20 cells each. C E_D-R_C and E_A-1/R_C plots for cells co-expressing the indicated plasmids. n ≥ 60 cells each.

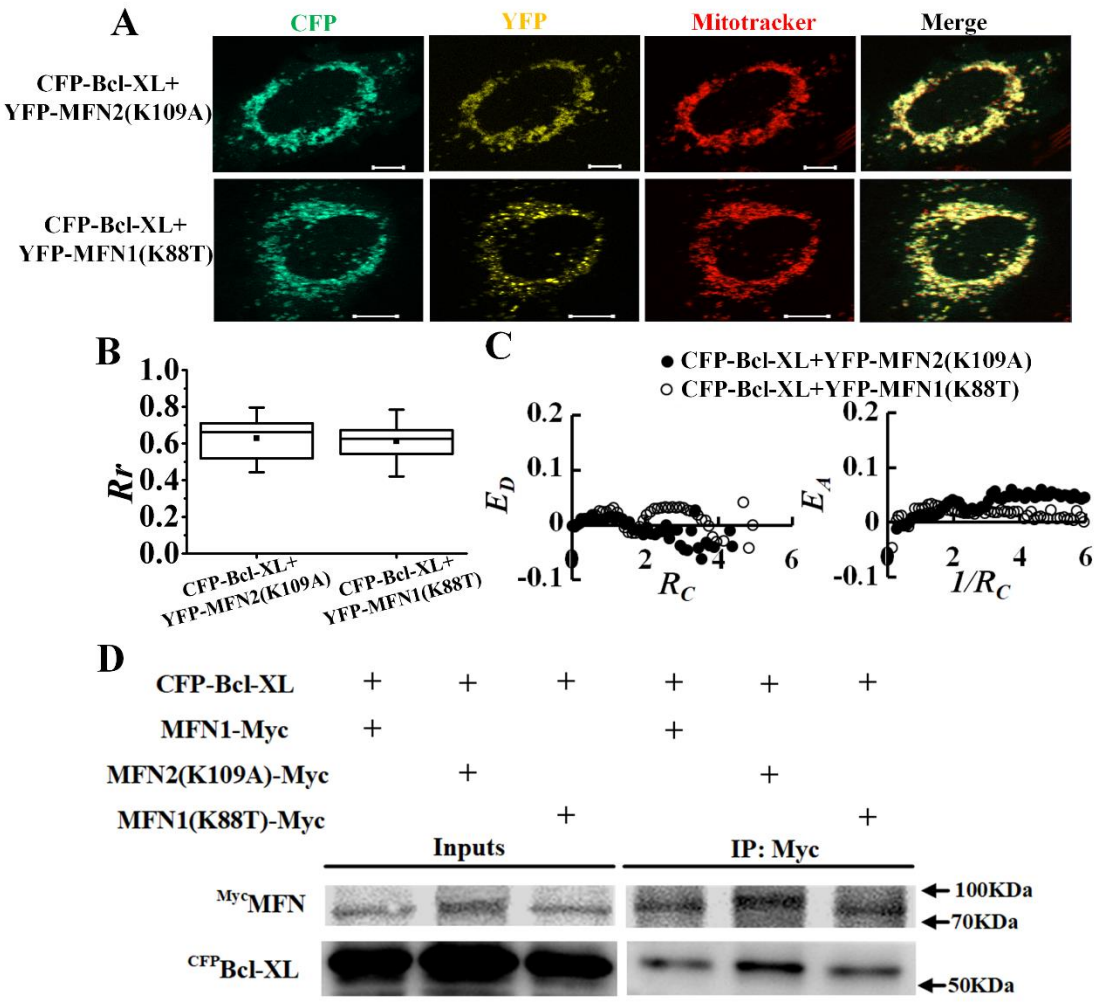

Fig. S4. Interaction between Bcl-XL and GTPase domain mutants of both MFN2 and MFN1 (MFN2(K109A) and MFN1(K88T)). A Fluorescence images of representative living Hela cells co-expressing CFP-Bcl-XL + YFP-MFN2(K109A), CFP-Bcl-XL + YFP-MFN1(K88T), and the corresponding merge images. B Statistical R_r values for the colocalization between Bcl-XL and MFN2(K109A), and between Bcl-XL and MFN1(K88T). n ≥ 20 cells each. C E_D-R_C and E_A-1/R_C plots for cells co-expressing the indicated plasmids. n ≥ 60 cells each. D Co-immunoprecipitation assay between Bcl-XL and MFN1/MFN2(K109A)/MFN1(K88T). Lysates prepared from Hela cells co-transfected with CFP-Bcl-XL and MFN1-Myc/MFN2(K109A)-Myc/MFN1(K88T)-Myc for 24 h subjected to immunoprecipitation with anti-Myc antibody, followed by anti-Myc and anti-CFP immunoblotting.